

AD-A255 511



TECHNICAL REPORT EL-92-26

2

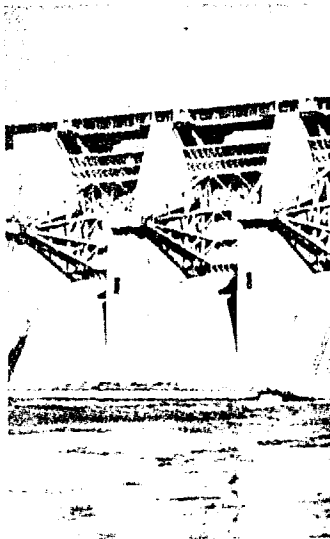
US Army Corps
of Engineers

DECIDUOUS FOREST SCENE COMPLEXITY IN HIGH-RESOLUTION MULTISPECTRAL SCANNER IMAGERY

by

Lee K. Balick

Multispectral Remote Sensing Department
EG&G Energy Measurements, Inc.
Mail Stop H-02, P.O. Box 1912
Las Vegas, Nevada 89125



DTIC
ELECTE
SEP 10 1992
S A D

92-24906



Handwritten scribbles and markings



August 1992

Final Report

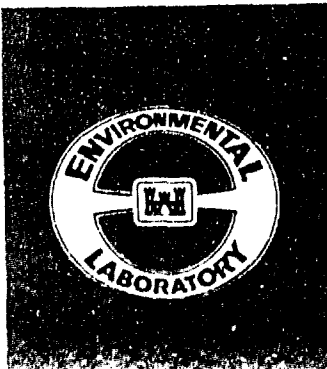
Approved For Public Release; Distribution Is Unlimited

92 9 09 009

Prepared for DEPARTMENT OF THE ARMY
US Army Corps of Engineers
Washington, DC 20314-1000

Under DA Project No. 4A162719AT40
Task BO, Work Unit 063

Monitored by Environmental Laboratory
US Army Engineer Waterways Experiment Station
3909 Halls Ferry Road, Vicksburg, Mississippi 39180-6199



Destroy this report when no longer needed. Do not return
it to the originator.

The findings in this report are not to be construed as an official
Department of the Army position unless so designated
by other authorized documents.

The contents of this report are not to be used for
advertising, publication, or promotional purposes.
Citation of trade names does not constitute an
official endorsement or approval of the use of
such commercial products.

REPORT DOCUMENTATION PAGE			Form Approved OMB No. 0704-0188	
Public reporting burden for this collection of information is estimated to average 1 hour per response, including the time for reviewing instructions, searching existing data sources, gathering and maintaining the data needed, and completing and reviewing the collection of information. Send comments regarding this burden estimate or any other aspect of this collection of information, including suggestions for reducing this burden, to Washington Headquarters Services, Directorate for Information Operations and Reports, 1215 Jefferson Davis Highway, Suite 1204, Arlington, VA 22202-4302, and to the Office of Management and Budget, Paperwork Reduction Project (0704-0188), Washington, DC 20503.				
1. AGENCY USE ONLY (Leave blank).	2. REPORT DATE August 1992	3. REPORT TYPE AND DATES COVERED Final report		
4. TITLE AND SUBTITLE Deciduous Forest Scene Complexity in High-Resolution Multispectral Scanner Imagery			5. FUNDING NUMBERS TA BO WU 063 PR 4A162719AT40	
6. AUTHOR(S) Lee K. Balick				
7. PERFORMING ORGANIZATION NAME(S) AND ADDRESS(ES) Multispectral Remote Sensing Department EG&G Energy Measurements, Inc. Mail Stop H-02, P.O. Box 1912 Las Vegas, NV 89125			8. PERFORMING ORGANIZATION REPORT NUMBER	
9. SPONSORING / MONITORING AGENCY NAME(S) AND ADDRESS(ES) U.S. Army Corps of Engineers, Washington, DC 20314-1000 U.S. Army Engineer Waterways Experiment Station Environmental Laboratory, 3909 Halls Ferry Road Vicksburg, MS 39180-6199			10. SPONSORING / MONITORING AGENCY REPORT NUMBER Technical Report EL-92-26	
11. SUPPLEMENTARY NOTES Available from National Technical Information Services, 5285 Port Royal Road, Springfield, VA 22161				
12a. DISTRIBUTION / AVAILABILITY STATEMENT Approved for public release; distribution is unlimited			12b. DISTRIBUTION CODE	
13. ABSTRACT (Maximum 200 words) This report summarizes within-scene variability and spectral relationships of high-resolution, multitemporal, multispectral scanner images of a deciduous forest in eastern Tennessee. The data were obtained using a helicopter-mounted Daedalus D-1268 multispectral scanner with a 1.25-milliradian instantaneous field of view at 175 ft (53.34 m) above ground level (agl) and 350 ft (106.7 m) agl. Flights were made under generally clear skies at predawn twilight, midmorning, and near solar noon in the north and west direction at both altitudes. In the midmorning and solar noon data, spectral bands of yellow-green, red, near-infrared, and thermal infrared energy were analyzed. Additional thermal infrared data from a Daedalus D-1261 scanner flown at 150 ft (45.7 m) agl under overcast skies were also available. Within-scene variability was analyzed to extract parameters for auto-regression models of texture for scene modeling and to provide validation data for physically based models of remotely sensed temperature variation of forests. <p style="text-align: right;">(Continued)</p>				
14. SUBJECT TERMS Coherence length Histogram Correlation function Multispectral imagery Forest canopy			15. NUMBER OF PAGES 84	
			16. PRICE CODE	
17. SECURITY CLASSIFICATION OF REPORT UNCLASSIFIED	18. SECURITY CLASSIFICATION OF THIS PAGE UNCLASSIFIED	19. SECURITY CLASSIFICATION OF ABSTRACT	20. LIMITATION OF ABSTRACT	

13. (Concluded)

The standard deviation, one-dimensional normalized autocorrelation functions, and coherence lengths of those functions were used to characterize the variability of images. The standard deviations of all channels increased with time (sun elevation) under clear conditions and, in the thermal channel, increased from about 1.0 °C at predawn twilight to 1.5 °C at midmorning, to 2.0 °C at solar noon. One-dimensional autocorrelation functions varied highly within images. Histograms of coherence lengths showed that they commonly vary over a factor of 10 within an image. The largest coherence lengths were from the near-infrared channel in the daytime under clear sky conditions. In the thermal infrared, coherence lengths were shortest in predawn twilight and longest in midmorning under clear skies. Coherence lengths for thermal imagery in overcast conditions were short. View (flight) direction differences, particularly in the thermal infrared band, were observed at solar noon but not midmorning.

Relationships between pixels in the thermal infrared and the reflected energy channels data were examined using multivariate least square regression. Using the correlation coefficient squared (r^2) as a measure of the quality, the relationships were never excellent, but the midmorning relationships were much stronger than at solar noon. Midmorning r^2 values were typically about 0.6 while the solar noon values were typically about 0.3. Midmorning relationships seemed simpler, and the best correlation of the thermal data were with the near-infrared and the sum of the three reflectance channels. At solar noon, the best correlation was with channels 5 and 3 which are strongly absorbed by green vegetation. Three-dimensional histograms were developed to try to separate the effects of shadowing and of green leaf area in the regression. However, these were not successful. Curiously, the distribution of data along a greenness index (near-infrared to red ratio) axis showed a strong shift of skew during the day indicating a shift of the color of the canopy between the two observation periods.

Accession For	
NTIS CRA&I	<input checked="" type="checkbox"/>
DTIC TAB	<input type="checkbox"/>
Unannounced	<input type="checkbox"/>
Justification	
By _____	
Distribution /	
Availability Codes	
Dist	Avail. and/or Special
A-1	

THIS QUARTER INSPECTED 1

PREFACE

This study was conducted as part of the U.S. Army Corps of Engineers Research Program "Electromagnetic Target Surround Characteristics in Natural Terrains." Funds for this study were provided by the Headquarters, U.S. Army Corps of Engineers, under Department of Army Project No. 4A162719AT40, Task B0, Work Unit 063. Additional support was provided by the U.S. Department of Energy, Department of Nuclear Safety, under Contract DE-AC08-83NV10282.

This study was performed under contract to Dr. Lee K. Balick, Multispectral Remote Sensing Department, EG&G Energy Measurements, Inc., Las Vegas, NV. Airborne imagery data acquisition was performed by Dr. David Hawley, Mr. Gary Menkel, and Mr. Victor Young of the Data Acquisition Section of EG&G Energy Measurements, Inc., Multispectral Remote Sensing Department (EG&G/EM/MRSD). Mr. John Brown was the pilot. Ground data acquisition was performed by Dr. Boyd Hutchinson, Dr. Dennis Baldocchi, and Mr. Russel Martin of the Atmospheric Turbulence and Diffusion Division, Environmental Research Laboratories, National Atmospheric and Oceanic Administration in Oak Ridge, TN. Field data assistance and equipment were provided by Mr. Alfonso Vasquez of the Environmental Laboratory (EL), U.S. Army Engineer Waterways Experiment Station (WES). Dr. James A. Smith of the Earth Resources Division, Terrestrial Physics Laboratory, at the NASA Goddard Space Flight Center provided essential interaction and motivation. Mr. Ed Doak of EG&G/EM/MRSD Data Analysis Section wrote the computer program to compute the one-dimensional autocorrelation functions and created the autocorrelation images. Mr. Harry Reid of the University of Nevada, Las Vegas, Environmental Research Center, performed most of the image processing, graphics, and data analysis tasks. Dr. Richard A. Weiss, EL, WES, served as contract monitor.

The study was performed under the general supervision of Dr. John Harrison and Dr. John W. Keeley, Director and Assistant Director, respectively, of EL, and Dr. Victor Lagarde III, Chief, Environmental Systems Division, EL; and under the direct supervision of Mr. Malcolm P. Keown, Chief, Environmental Constraints Group (ECG), EL.

At the time of publication of this report, Director of WES was Dr. Robert W. Whalin. Commander and Deputy Director was COL Leonard G. Hassell, EN.

This report should be cited as follows:

Balick, Lee K. 1992. "Deciduous Forest Scene Complexity in High Resolution Multispectral Scanner Imagery," Technical Report EL-92-26
U.S. Army Engineer Waterways Experiment Station, Vicksburg, MS.

CONTENTS

	<u>Page</u>
PREFACE	1
LIST OF TABLES	4
CONVERSION FACTORS, NON-SI TO SI (METRIC) UNITS OF MEASUREMENT	5
PART I: INTRODUCTION	
Background	6
Objectives and Scope	9
PART II: DATA	11
Study Site	11
Instrumentation	12
Acquisitions	14
PART III: ANALYSES	17
Subsectioning	17
Variance and Coherence Lengths	17
Spectral Relationships	18
PART IV: RESULTS AND DISCUSSION	21
Variance and Coherence Length	21
Autocorrelation and Coherence Length	22
Spectral Relationships	28
PART V: CONCLUSIONS AND RECOMMENDATIONS	31
Variance and Autocorrelation	31
Spectral Relationships	33
REFERENCES	35
FIGURES 1-45	

LIST OF TABLES

<u>No.</u>		<u>Page</u>
1	Spectral Band Characteristics	12
2	Selected Flight Line Times, Direction, and Sun Angles	15
3	Image Digital Number Means and Standard Deviations	21
4	Coherence Length Distribution Summary Statistics	25
5	Summary of Spectral Regression Relationships	28

CONVERSION FACTORS, NON-SI TO SI (METRIC)
UNITS OF MEASUREMENT

Non-SI units of measurement used in this report can be converted to SI
(metric) units as follows

<u>Multiply</u>	<u>By</u>	<u>To Obtain</u>
degrees (angle)	0.01745329	radians
feet	0.3048	meters

DECIDUOUS FOREST SCENE COMPLEXITY IN HIGH-RESOLUTION
MULTISPECTRAL SCANNER IMAGERY

PART I: INTRODUCTION

Background

1. Modeling complex scenes requires the estimation of nonspatial characteristics such as pixel brightness mean, variance, and frequency distribution, as well as the spatial arrangement of scene-brightness variations. Specific scene component or segment (an area of the scene with generally uniform properties such as an area of forest, a patch of bare soil, or a road which would be modeled separately from other regions of the image) characteristics change with environmental conditions such as atmospheric conditions and sun angle as well as viewing attributes like view direction, sensor angular resolution, the area of a pixel, atmospheric effects, and sensor noise. Our knowledge of reflectance processes and the factors controlling them is fairly advanced. Predicting average radiant exitance in the visible and near-infrared wavelengths is well developed from both practical and theoretical perspectives for many natural and cultural scene components (Smith 1983; Strahler, Woodcock, and Smith 1986). The modeling of thermal radiant exitance is less well developed, but models exist for many scene components (Smith 1983). The variance, the spatial arrangement of the variance, and the way these change with environmental and viewing conditions are complicated and less well understood. Consequently, variations of the average pixel brightness for most natural or background scene components are often simulated with statistical models using arbitrary or empirically derived parameter values (Haralick 1979; Faugeras 1980; Botkin et al. 1981; Rosenfeld 1981; Ahuja and Schachter 1982; Ben-Yosef, Rajat, and Feigin 1983; Loefer et al. 1983; Finlay, Weathersby, and Gaby 1983; Ben-Yosef et al. 1986).

2. The concept of scene complexity includes such a wide range of scene characteristics that it is difficult to define succinctly. Intuitively, it is related to the magnitude, frequency distribution, and spatial organization of pixel brightness in an area. The area can be a scene (whole image) or a scene component (image segment). Magnitudes and variations are described by frequency distributions (or their parameters), but the description of spatial relationships is more difficult. The list of spatial characteristics

comprising scene complexity is long and includes directionality, stationarity, autocorrelation, patchiness, edge strength, number of objects or edges per unit area, number of different shapes, structured versus random variance, etc. In practice, only a subset of these characteristics applies to a particular application so that workable problem-oriented definitions can be made. For reasons discussed later, the emphasis of this report is placed on examining the variability and the one-dimensional autocorrelation function as measures of scene complexity (the magnitude, variability, and spatial organization of pixel brightness) in high-resolution, multispectral (visible, near-infrared, and thermal infrared) scanner images of a deciduous forest.

3. Forests cover large areas of the earth's surface, and forests or trees can be expected to be a part of the environment of most tactical situations in temperate and tropical climates. Models of average bidirectional reflectance and directional average radiant temperature of vegetation for remote sensing applications have been developed and applied to forest situations (Strahler and Li 1981; Otterman 1984; Smith et al. 1981a, Baldocchi et al. 1985; Baldocchi et al. 1986; Li and Strahler 1986). With few exceptions, the canopy structure is represented by spatial averages of parameters like leaf area index and leaf inclination angle distributions. Therefore, these models are directly applicable at resolutions where several trees are within a pixel, the usual case in data from civilian satellites. Except for the Kimes and Kirchner (1982) three-dimensional model (which is more of a research than an applications model), they are not useful for simulating texture induced by individual trees or tree parts when they can be resolved by the imaging system. This is frequently the scale of image texture in data obtained from aircraft photography and airborne electronic imaging systems. While allowance is made for stem, bark, and ground reflectance in some models, it is spatially averaged. Individual trees of forest openings and edges are not considered. (Again, the Kimes and Kirchner (1982) model may be an exception.) Thermal infrared models do not distinguish between the woody parts of trees and leaves (Smith et al. 1981a, Smith 1983), which can have large energy budget and temperature differences. There seem to be no published physically based models useful for image modeling applications that simulate spatial variations of either reflected or emitted radiant exitance of forests at scales where the individual trees or tree structure can be resolved.

4. The need for such models arises, in part, from military requirements to characterize the complexity of target backgrounds and to simulate the

conditions in which electromagnetic sensor systems are expected to operate. Scene simulation software systems have been and continue to be developed for a number of sensor types and in several regions of the electromagnetic spectrum. These systems require mean radiances or temperatures and a way of estimating texture for a variety of scene components under differing environmental and viewing conditions. To fill this need for deciduous forests in the visible, near-infrared, and thermal infrared spectral regions, field measurement and modeling studies were initiated by the Environmental Laboratory of the U.S. Army Engineer Waterways Experiment Station (WES). The modeling research was oriented to temperature modeling for thermal infrared scene simulation. Also, it was recognized that many of the techniques might be applicable to reflectance modeling since the insulation, canopy structure, and view calculations were the same. The thermal model development was designed to be an extension of Smith et al. (1981a) by allowing the forest canopy to have a rough or irregular shape which allows for spatially variable solar absorption and viewing geometry. The model would then produce estimates of the mean, variance, and coherence length of temperature for canopy height transects through a forest as functions of the relevant environmental conditions, canopy top geometry, and view angle. While an extension of the spatially averaged model, it would still apply to closed canopies with uniform stomatal function and would not simulate woody material or ground temperatures nor the heat transfer or storage in them. The field measurement program was designed to obtain the data necessary to drive the thermal model (or other models), investigate specific model assumptions, and provide imagery for model validation studies including characterizing the means, variances, and coherence lengths under a variety of illumination and view situations. Providing these numbers would also assist implementation of statistical algorithms in use at WES.

5. As mentioned, the parameters applied in some of the thermal infrared scene simulations at WES use the mean, variance, and coherence length (the distance where the autocorrelation function decreases to a value of $1/e$ from a value of 1.0 at distance of zero) of temperature within a scene component to assign radiance values to pixels. The values are calculated with a simple two-dimensional autoregression model using the one-dimensional coherence length as the spatial parameter in each direction of the array. The coherence lengths can be different in any direction, but in practice they are usually assumed to be isotropic. The result is a stationary, two-dimensional array of temperatures with the specified mean and variance and with exponentially

decreasing isotropic autocorrelation. There are no features in the autocorrelation function, such as plateaus or local maxima, and therefore no pattern or shape. The assumptions about the autocorrelation allow for efficient texture modeling at a level of sophistication above using a Gaussian model. How valid are these assumptions for a forest at resolutions where individual trees and parts of trees are well resolved and when irradiance is either weakly or strongly directional? This can be an important question for both physically and statistically based texture and pattern modeling for many applications.

6. Relationships between images of different parts of the electromagnetic spectrum are of traditional interest in remote sensing science. The data used to examine within-image variability and autocorrelation can also be employed to examine the relationships between the images of the emitted thermal infrared energy and reflected solar energy. Of more specific interest is the fact that one of the basic assumptions of the aforementioned thermal infrared model is that differential irradiance of the canopy, caused by the shape of the canopy top and the position of the sun, is a major cause of spatial variation of forest canopy temperature. This would be observed as a strong correlation between temperature, solar energy absorbed, and thus irradiance. Also of practical interest is the possibility of using reflected energy images to approximate properties of thermal images for image-modeling applications where physical modeling is not feasible. An early step in defining these relationships is a statistical analysis of pixel-by-pixel variance of multispectral data. For this report, a multivariate least-squares regression of reflected pixel values on radiant temperatures is performed to describe the overall relationships between these energy regimes.

Objectives and Scope

7. This report summarizes a set of high-resolution, multitemporal, multispectral scanner imagery of a mixed-species deciduous forest in summer. Within-image pixel variability and one-dimensional autocorrelation functions are used to characterize individual images for a limited range of irradiance and viewing geometries. By doing so, the parameters for autoregression modeling of forest texture are determined, and validation data for physically based models are made available. Additionally, relationships between spectral bands are explored with emphasis on the correlation between the emitted thermal infrared energy and the reflected visible and near-infrared energy. This

helps to examine and evaluate the hypothesis that variations of remotely sensed temperature are due, in part, to variations of irradiance and shadowing on the rough canopy top.

8. The images are a part of the data obtained during a field measurement program conducted in June 1986 near Oak Ridge, Tennessee. Other data, which will be presented as appropriate in future reports, include airborne oblique (low depression angle) video thermal imagery and aerial color photographs at multiple view and sun angles; ground-based radiant temperature measurements of foliage, tree stems, and the forest floor; the radiant energy fluxes above and within the forest; and meteorological data above and within the canopy. Some of the ground-based measurements are used in this report to support interpretation of the scanner image features. However, the work presented here is focused on the scanner image data and its spatial and spectral characteristics as irradiance and viewing geometry change.

PART II: DATA

Study Site

9. Data were obtained at the Forest Meteorology research site operated by the Atmospheric Turbulence and Diffusion Division of the National Oceanic and Atmospheric Administration's Environmental Research Laboratory near Oak Ridge, Tennessee. The site is on a gently sloping spur ridge (about 3 percent slope) at about 365 m above mean sea level. The forest at this site consists of an uneven-aged mixed-species stand about 40 years old and is typical of oak-hickory forests in the Appalachian region. Overstory species are predominantly oaks but with a significant presence of red maple and tulip poplar in the area. In 1976, the average tree height was 21.5 m with a basal area of about 26 m²/ha. Leaf area indices are about 3.8 for the overstory and 1.1 for the subcanopy while the woody area index is about 0.6; the total plant area index is 5.5. Mean leaf inclination angles are 10, 20 and 38 deg* in the subcanopy, the overstory below crown closure and the overstory above crown closure, respectively. A detailed description of this site is given by Hutchison et al. (1986).

10. Two instrumented research towers are visible in the images. The tallest is a 44-m aluminum walk-up tower with a platform at the top. The second is a 33-m steel tower roughly to the west-southwest of the large tower (108 deg west of north). Two instrument packages suspended on cables between the towers and tower guy lines are also visible in many of the images.

11. Hutchison and Matt (1977) report the probability of gap (direct line of sight) as a function of elevation angle for three depths in the canopy. These data also describe the probability of line-of-sight in the canopy as a function of nadir angle and the penetration of direct insolation as a function of the sun's zenith angle for the reported depths in the canopy. At a height near crown closure, the probability of gap is 0.8 or greater in the nadir angle range of 20 to 55 deg with rapid decreases with angle in both directions. At the forest floor, probabilities are on the order of 0.1 or 0.2 for nadir angles less than 55 deg decreasing to 0 at about 72 deg. Other studies of the radiant energy budget of this forest indicate that the

* A table of factors for converting non-SI units of measurement to SI (metric) units is presented on page 5.

probability of gap at the forest floor at nadir is about 0.1 (Smith et al. 1981b, Baldocchi et al. 1984). Forest openings are not considered in these studies, but other data (Baldocchi et al. 1984) and photographs indicate that these values have large spatial variability. Hemispherical photographs of this forest are published in Hutchison and Matt (1977), Baldocchi et al. (1985), and Baldocchi et al. (1986).

Instrumentation

12. The primary source of image data is a Daedalus D-1268 multispectral scanner. The scanner was mounted on a helicopter equipped with a microwave altimeter. The scanner was operated in the "half angle" mode giving a 1.25-milliradian instantaneous field of view (IFOV) scanning across approximately 22.5 deg either side of nadir at 100 scans per second. The scanner was operated at 175 and 350 ft above ground level (agl). This gives instantaneous resolutions at nadir of 0.22 ft at an altitude of 175 ft agl and 0.44 ft at 350 ft agl. Near the top of the canopy, at 66 ft above the forest floor, resolutions at nadir are 0.14 and 0.36 ft, respectively. Ten reflectance spectral bands and one thermal infrared band are available, but since much of the reflectance information is redundant and some is of lesser interest, three reflectance bands commonly used in vegetation studies and the thermal band are selected for analysis. These bands are given in Table 1.

Table 1
Spectral Band Characteristics

Channel No.	Wavelength Band microns	Physical Characteristics
3	0.53 - 0.60	Yellowish green, reflected, strong leaf absorption but in green reflectance peak
5	0.63 - 0.69	Red, reflected, strong chlorophyll absorption
7	0.76 - 0.90	Near-infrared, reflected, low leaf absorption and high leaf scattering
12	8.50 - 14.0	Thermal infrared, primarily emitted

13. The reflected energy channels (3, 5, and 7) were uncalibrated, and no suitable reference surfaces were present within the image. Therefore, the

analyses were performed on data in arbitrary scanner units of eight-bit digital numbers (DNs) ranging from 0 to 255. Because the data were not in physical units in these channels, the mean and variance statistics depend on instrument settings of gain and offset in each channel. Gain settings were different for each band but were not changed between flights.

14. The thermal infrared channel has internal blackbody references permitting conversions of DN's to temperature units. For this study, a value of 1 DN is equivalent to 0.1 °C, but the actual values presented are DN values. A problem which has not yet been fully diagnosed exists in this channel. Horizontal (scan direction) striping caused by shifts of entire scan lines is present (shifts are occasionally on the order of 10 DN's). Inspection of the data suggests that the absolute values of the DN's within a scan line are suspect but that the differences within a scan line are valid (except in the usual case where data are saturated). For the quantitative analyses, a constant was added to each scan line to give it a mean value of zero. Thus, even though the mean values are not valid, variance and autocorrelation functions within scan lines are valid and comparable to other scan lines.

15. Some additional thermal infrared imagery was obtained using a modified Daedalus D-1260 (D-1261) scanner with the same geometrical and spectral characteristics as the D-1268. These data also have an undiagnosed noise problem more subtle than line-brightness shifting. Quantitative analyses of these data are suspect, and only a minimal amount is reported. These images are of interest because they were obtained under overcast sky conditions.

16. Scanning geometry causes changes of pixel size and spacing with distance from nadir. Digital aircraft scanner data are often adjusted by inserting pixels of interpolated DN's as needed to correct this panoramic distortion. No such modifications were applied to the data used in this study for two reasons. First, the scan angle was restricted to 22.5 deg from nadir instead of the usual 45 deg. Panoramic distortions increase geometrically with nadir angle and remain small within 22.5 deg. Secondly, the analyses were restricted to the central 512 pixels, further reducing the effective maximum nadir angle to slightly over 16 deg. As a result, only 6 pixels would be inserted in 256 on each side of nadir. Since some error is inherent in the correction, applying it did not seem beneficial.

Acquisitions

17. Three sets of flights were made with the Daedalus D-1268 multi-spectral scanner on June 16, 1987: predawn twilight, midmorning, and solar noon. Each set consisted of a series of flights along east-west and north-south lines over the large tower at each of 175 and 350 ft agl. On June 10, the D-1261 scanner was flown at a single elevation of 150 ft agl. The pilot attempted to center the flight line over a large instrumented tower extending well above the canopy and serving as a locational reference within the imagery. Because of the helicopter movement, rotor-generated turbulence did not effect the canopy until after it was scanned. A set of flights took about half an hour to complete, but individual flight lines took about 1 min. One pair of east-west and north-south flight lines at each altitude was selected for analysis. Selected flight times, directions, solar elevation, and solar azimuth angles are given in Table 2. June 16, 1986, had clear skies in the morning with cumulus clouds forming during the midday flights. Though no cloud shadowing of the study area occurred during the flight, more subtle cloud effects are possible at the end of the experimental period. Two sets of flights were made on June 10 and 11 which were overcast at flight times. All flights provide thermal infrared imagery; only the daytime flights on June 16 provide visible and near-infrared data (channels 3, 5, and 7).

18. Slight variations of helicopter flight speed, pitch, and yaw (roll is corrected by scanner system) cause large uncertainties in the spatial relationships between scan lines. Thus the spatial properties of the data in the flight direction are unknown. Also, image-to-image registration is not feasible. Since scans were made in less than 0.01 sec, data within scan lines seemed unaffected by aircraft movement. Therefore, individual scans are considered to be separate measurements of variance and one-dimensional autocorrelation in the direction perpendicular to the flight direction.

19. Representative image data are shown in Figures 1-15. Figures 1-8 show several of the 2,048 by 512 data sets. Figure 1 contains thermal infrared data from west direction flights on June 10 and 11 acquired at 150 ft agl under overcast conditions. Temperatures are rather uniform and cool in the image on the left in Figure 1, and the image does not reproduce well. The two bright spots in the image are associated with instrumentation. Some of the data acquired on June 16 are shown in Figures 2-8; Figure 2 is twilight thermal infrared data acquired at 350 ft agl; Figures 3 and 4 are midmorning west

Table 2
Selected Flight Line Times, Direction, and Sun Angles

Date	Time	Elev.	Flight	Solar Azimuth	Solar Elevation
June	(EST)	ft agl	Direction	(clockwise from north)	deg
1986					
16	0550	175	West		
16	0554	175	North		Predawn
16	0604	350	West		twilight
16	0607	350	North		
16	0931	175	North	87	36
16	0934	175	West	87	36
16	0942	350	North	89	38
16	0945	350	West	89	39
16	1331	175	North	176	77
16	1349	175	West	199	77
16	1353	350	North	202	76
16	1356	350	West	204	76
11	0943	150	North	89	38
11	0944	150	West	89	39
10	1343	150	North	193	77
10	1345	150	West	196	77

direction flights acquired at 350 and 175 ft agl for channels 12 and 7, and Figures 5-8 show the corresponding data at solar noon plus channels 5 and 3. The images have not been enhanced. The bright areas in the thermal infrared images in Figure 5 are sunlit areas of the forest floor. Channels 5 and 3 are very dark and qualitatively illustrate differences in overall canopy reflectance (differing detector responses have not been taken into account). Bright areas in these channels are the tower, instrumentation, and, in channel 5, sunlit areas in the forest floor. Both towers and the instrumentation suspended between them are clearly visible in the lower right areas in the images on the right side of Figures 7 and 8. A few bright areas in Figure 8 not related to instrumentation are probably facilities beneath the canopy. The images in Figures 1-8 were reduced by a factor of 16 to fit on a 512- by 512-pixel display. Subsections at full 512 by 512 resolution with the tower at the top are shown in Figures 9-15. Instruments and cables are clearly visible in these images. Figure 9 contains thermal infrared data acquired at 150 ft agl and corresponds to the data on the right of Figure 1. Twilight thermal infrared data acquired on June 16 at 350 ft agl and corresponding to Figure 2

are shown in Figure 10. Figures 11-13 are subsections acquired at midmorning at 175 ft agl from channels 12, 7, and 5, respectively. Figures 14 and 15 are subsections of thermal infrared data obtained at 350 ft agl in each of the flight directions.

PART III: ANALYSES

Subsectioning

20. Since each of the daytime flights on June 16 resulted in 4 images, 40 images were being analyzed. In order to sample roughly the same areas and to reduce the volume of data, steps were taken to subsection the images and to reduce sample sizes. First, 2,048 by 512 subsections were taken. In the scan direction, the central 512 pixels were used to minimize geometric and directional effects. The large meteorological tower was centered in the flight direction. Next, every eighth scan line was selected to reduce the number of scan lines to 256, a convenient number for image processing. Regular sampling added some independence between sampled scans and helped ensure that the length of the 2,048 line images was represented. To perform the statistical analyses, scan lines which included the tower or other instrumentation were removed. This reduced the data sets to roughly 210 scan lines (range is 181 to 239). Spatial information was not needed to examine spectral relationships, so every fourth pixel in a scan line was used giving a sample size on the order of 25,000 pixels per image.

Variance and Coherence Lengths

Image variance

21. The variance of DNs for each scan line unaffected by the tower or instrumentation was calculated and averaged for each subsectioned image.

Autocorrelation and coherence length

22. The analysis of one-dimensional autocorrelation functions and the subsequent extraction of coherence length is considerably more involved than computing variances. The first step was the creation of an image of one-dimensional autocorrelations for each data image. Coherence lengths for each scan line unaffected by the tower were extracted, and their frequency distributions were examined. Additional details are given in the following paragraphs.

Calculation of autocorrelation functions

23. One-dimensional autocorrelation functions were computed for each scan line in the 256 by 512 image subsections. The autocorrelation function describes the correlation of pixel DN values as a function of distance or lag.

The unit of distance is the sampling interval or, in this context, pixels, and is the same as the nominal values of the IFOV described above. A command file of IDIMS (Interactive Digital Image Manipulation System produced by the Environmental Systems Laboratory, a division of TRW, Inc.) image processing functions was developed to perform the following tasks: for each scan line, a constant was added so that the mean DN of each line was zero. Then the discrete one-dimensional Fast Fourier Transform (FFT) was taken, multiplied by its complex conjugate, and the inverse FFT performed. Assuming symmetry about the distance of zero, only the values at zero and positive distances were kept. These values were then normalized by dividing the value at a distance (lag) of zero so that the correlation at a lag of zero was always 1.0 and the autocorrelation function could then range from 1.0 to -1.0. As the calculations proceeded on a line-by-line basis, a new image was created containing the autocorrelation values. This real-valued image with a range of -1.0 to 1.0 would not display on monitors which usually require byte data in the range of 0 to 255. Therefore, a second autocorrelation image was created for display by multiplying by 100, adding 100, and converting to byte data. This mapped the real -1.0 to 1.0 data to 0 to 200 byte data and generated the autocorrelation images given in the figures. The real-valued images, scaled from -1.0 to 1.0, are the data used in the statistical analyses.

Coherence length frequency distributions

24. The coherence length is defined here as the distance or lag where the autocorrelation function decreases to a value of $1/e$ (0.37). Its origin lies in modeling spatial processes where interactions decrease, or are assumed to decrease, exponentially with distance. In image texture modeling, this assumption can simplify mathematical simulations. A viewing of the autocorrelation length images revealed that the value of the coherence length varied considerably within images. To characterize its variability, a histogram of coherence lengths for each image was calculated.

Spectral Relationships

Regression

25. There is somewhat of a paradox here: values proportional to reflectance are assumed also to be proportional to absorptance within the spectral band. The validity of this assumption relies on the fact that foliage (or nonfoliar materials) reflecting relatively large amounts of light

is receiving relatively large amounts of light and therefore is also absorbing relatively large amounts of energy. Sunlit leaves are generally warmer than shaded leaves, but the assumption that reflected light is proportional to absorbed light is not strictly correct. Also, daytime leaf temperatures are strongly influenced by transpiration which is, in turn, strongly controlled by stomatal function. Stoma respond in complex ways to several environmental factors, including light, that vary within the canopy and in time. Stomatal response to light tends to weaken the relationships between irradiance and temperature. Another problem is that most pixels contain mixtures of materials. While leaves comprise most of the image, they have differing orientations and exposures to the sun, sky, and airflows. Different species, possibly even different individuals within a species, have different stomatal responses to light and thus different temperatures. Additionally, the canopy is not opaque. Woody stems, branches, and the forest floor are partially visible through the tree crowns and canopy openings exit in the image. These components may be directly illuminated, or they may be shaded. Most of the nonfoliar materials have different thermal response times and heat storage characteristics further complicating the relationships between irradiance and temperature. Nevertheless, if thermal variations could be predicted from variations of reflected light with adequate reliability, this might prove to be a practical way of estimating thermal infrared image texture. An examination of relationships between changes of reflected light and temperature are of both theoretical and practical interest.

26. Regression relationships are developed to predict (correlate) thermal infrared pixel values with the values of the reflected energy channels. Seven independent variables were the DNs from channels 3, 5, and 7 (DN3, DN5, and DN7), their squares ($DN3^2$, $DN5^2$, and $DN7^2$), and their sum (SUM). If any pixel was saturated (had a DN value of 0 or 255) in any channel, it was eliminated. The mean was subtracted from each variable for the regression calculations. Regression equations for each possible combination of independent variables was computed for each of the eight daytime multispectral flights using the procedure RSQUARE in the SAS statistics software package (SAS Institute 1987).

Spectral histograms

27. Because the relationship between the thermal and reflectance channels changed over time and was relatively weak, some exploratory statistics were generated in the form of two types of three-dimensional histograms. One

was frequency of combinations of DN12 and DN5 values, and the second was frequency of combinations of the ratio DN7/DN5 and DN12. DN5 was used as a measure of direct solar irradiance, so the DN5-DN12 histogram was generated to provide more detail in the relationship between temperature and irradiance. The DN7/DN5, or near-infrared to red ratio, is often used as an index "greenness" or of green vegetation quantity. Therefore, this histogram was developed to try to show more detail on temperature differences related to the amount of leaf in the pixel. Some caution is appropriate here. The color of light changes with depth in the canopy as the shorter wavelengths (DN5) are absorbed more rapidly than the near-infrared (DN7). The DN7/DN5 ratios from shaded areas of the image or from deep within the canopy may not respond to foliage the same way as the directly illuminated foliage. Additionally, at least for the average canopy, the directional reflectance properties of each channel change differently with solar elevation thus changing the ratio of the channels.

PART IV: RESULTS AND DISCUSSION

28. The data and analysis results are presented in pictorial, graphical, and tabular formats. While the analyses were performed on all the data described earlier, representative subsets of the pictorial and graphical results have been selected to best illustrate differences or the lack of differences as imaging and environmental conditions change. Variations within single band images are considered before the spectral relationships. Within the image, variance is characterized first. Then the one-dimensional auto-correlations are presented in pictorial format, followed by coherence length characteristics in pictorial and tabular formats. Lastly, relationships between the thermal infrared pixels and those of reflected light, as described by regression equations and histograms, are given.

Variance and Coherence Length

29. The average scan line DN means and standard deviations for each image are given in Table 3. Several of the data characteristics are important for interpreting these numbers. First, because the detectors for the

Table 3
Image Digital Number (DN) Means and Standard Deviations (S)

Time (EDT)	Dir.	Elev. ft agl	Ch. 12		Ch. 7		Ch. 5		Ch. 3	
			Mean DN	S DN	Mean DN	S DN	Mean DN	S DN	Mean DN	S DN
0554	N	175	62.4	8.0						
0550	W	175	70.4	8.3						
										(predawn)
0607	N	350	62.0	8.3						
0604	W	350	66.4	8.5						
0931	N	175	110.1	14.9	80.1	30.3	48.1	10.2	37.0	15.1
0934	W	175	107.6	13.8	80.6	28.8	48.3	10.1	37.1	14.9
0942	N	350	112.0	15.5	81.2	30.2	49.2	10.1	38.5	15.0
0945	W	350	113.6	15.3	83.8	30.2	49.6	10.2	39.0	15.0
1331	N	175	147.3	20.8	157.4	41.5	71.9	15.7	75.7	23.9
1349	W	175	154.0	19.4	165.7	41.1	73.0	15.5	75.9	22.7
1353	N	350	151.1	22.7	164.2	42.1	75.3	16.5	78.7	15.1
1356	W	350	130.5	16.8	143.1	36.2	66.5	12.8	65.5	18.6

reflectance channels are not yet calibrated, physical interpretation of comparisons between reflectance channels are not valid. Secondly, the thermal infrared (channel 12) data are in units equivalent to 0.1 °C. However, it must be assumed that the whole-line brightness shifts are distributed symmetrically about zero in order for the thermal infrared means to be valid. It is not yet known whether this is an accurate assumption. (Scan line mean DNs were subtracted from individual pixels to calculate standard deviations of the channel 12 data.) Lastly, because of the noise characteristics of the sensor used on June 10 and 11, values for these flights are not given.

30. The standard deviation of radiant temperatures increased with sun angle from less than 1 °C at morning twilight to about 1.5 °C at midmorning to around 2.0 °C at solar noon. These increases were roughly proportional to increases of the mean. On the afternoon of a different day at the same site, Balick et al. (1987) observed somewhat different behavior with circular scanning radiometers suspended above the canopy with an IFOV on the order of 1 m: radiant temperature standard deviations did not change with solar elevations when the sun was higher than about 25 deg. (A rapid evening transition to nighttime conditions began when the sun was between 15 and 25 deg above the horizon, 1 to 2 hr before sunset.) Those standard deviations measured remained about 1 °C, about half that of the image data. This is likely due to the larger IFOV of the radiometers and/or their static location over a fairly uniform area. Like the thermal infrared, the reflected energy channels showed an increase of the standard deviation between midmorning and near solar noon. The increases were on the order of 25 percent for channel 7 and 50 percent for channels 5 and 3. Surprisingly, image variability does not change with scanner altitude. (The existence of directional viewing effects within scanner images was explored by comparing the means and variances of the 64 pixels on each edge of the 2,048 by 512 images for each flight line. No significant differences or patterns were found, and it appears that there are no view directional effects in the scan direction within the individual images used in this study.)

Autocorrelation and Coherence Length

Autocorrelation images

31. A representative selection of autocorrelation images is given in Figures 16-22. Short distances or lags (high frequencies) are toward the left

of the image with zero lag at the left edge always having an autocorrelation of 1.0 (or a value of 200 for the mapping used in the figures). Each row or line represents the one-dimensional autocorrelation function of a corresponding data scan line (every eighth line of the 2,048 by 512 images) out to a maximum lag of 256 pixels. Except for the predawn twilight data (top of Figure 16), the figures appear generally similar. It is important to note that the autocorrelation functions vary throughout the image. Extensions of high correlation to larger lags near the middle of the image in several of the figures (both parts of Figure 20 for example) are due to the tower. However, the effects of the tower, which are present in all images, are difficult to discern in other images such as in Figure 21. Extensions of relatively high correlation to moderate lags near the top or bottom of the images are attributed to forest characteristics, usually sunlit or shaded openings in the canopy. Examples of this can be found in the top parts of Figures 18 and 22.

32. Some of these autocorrelation images are presented again on the right sides of Figures 23-31 alongside the image data from which they were generated (every eighth line of the 2,048 by 512 images). The midmorning channel 5 image data of the forest in Figure 27 are low-valued and do not reproduce well, but they are not saturated. All autocorrelation values greater than $1/e$ (137 autocorrelation image brightness) were remapped to an image brightness of 200. Thus the coherence lengths are at the left-most interface between the remapped data and the original autocorrelation data. The irregularity of the coherence lengths throughout the images is apparent (except the predawn twilight thermal infrared image in Figure 23 where the larger coherence lengths are due to the tower and ground facilities under the forest openings). While the large coherence lengths can be associated with forest features, there is nothing extraordinary about these features; they can presumably be found to some degree in most natural forests. At this point, it seems difficult to select a representative one-dimensional autocorrelation function or coherence length for any of the daytime images. (It should be noted that autocorrelation functions are considerably different when the sky is overcast. In the June 11, 0944 EDT data, autocorrelation functions look very much like the predawn twilight data on June 16. The June 10, 1345 EDT data also tend to have relatively short coherence lengths, but there are many artifacts due to image noise.)

Coherence length frequency distributions

33. To gain a more quantitative understanding of the variability of coherence lengths, the frequency distributions for each flight were determined. Scan lines containing the tower or other instrumentation are not included. Figures 32-40 contain histograms of coherence length for the images in Figures 23-31. (There is varying scaling of the frequency axis, and coherence lengths greater than 50 pixels are plotted in the 50-pixel value bin.) It is clear in these figures that all the distributions are strongly skewed and many have a large range of values. However, quantitative comparison between the figures is difficult. For that reason, descriptive parameters summarizing the distributions for all of the images are given in Table 4.

34. One of the outstanding features of the data in Table 4 is the large range of coherence lengths within an image. The minimum and maximum frequently vary by a factor of 10. Even the 25th and 75th percentiles within an image often differ by a factor of nearly 3.

35. Coherence lengths for the predawn twilight thermal infrared images are considerably smaller than any of the daytime images. This is especially true for the middle percentiles, suggesting a frequency distribution of a different shape between daytime and nighttime imagery. Comparing the mean with the median value is another way to indicate this change. There is a factor of 2 difference for the twilight thermal images, whereas the ratio rarely exceeds about 1.4 in the daytime imagery. Otherwise, the midmorning mean and percentile coherence length values exceed those at near solar noon in the reflectance channels at the same flight altitude. This difference also exists in the thermal infrared data when flights of the same altitude and direction are compared.

36. The sampling interval in units of distance (or the distance per pixel) changes by a factor of 2 between the different flight altitudes. Thus, if the same processes were being completely sampled at both flight altitudes, the autocorrelation functions and the coherence length in units of pixels at 175 ft agl would be twice that obtained at 350 ft agl. However, while the sampling interval changes by a factor of 2, the sample size (IFOV or pixel area) changes by a factor of 4. As area averaging is done in two directions, this would tend to increase the difference between flight altitudes. The data in Figure 4 do not confirm either idealization. The twilight thermal data show almost no difference of distribution of coherence lengths between flight altitudes. The midmorning data do show a consistent difference but with a

Table 4
Coherence Length Distribution Summary Statistics

<u>Time/Dir Elev.</u>			<u>Coherence Lengths (pixels)</u>						
<u>Ch</u>	<u>(EDT)</u>	<u>ft</u>	<u>Mean</u>	<u>Percentiles</u>				<u>Min.</u>	<u>Max.</u>
				<u>25%</u>	<u>50%</u>	<u>75%</u>	<u>90%</u>		
12	0554N	175	1.7	0.9	1.0	1.3	3.6	0.8	19.0
12	0550W	175	2.1	0.9	1.2	3.1	4.1	0.8	12.7
12	0607N	350	2.1	0.9	1.0	2.1	4.0	0.8	25.0
12	0604W	350	2.5	0.9	0.9	3.1	7.0	0.7	22.7
12	0931N	175	11.8	8.2	10.6	14.2	19.3	4.0	33.4
12	0934W	175	11.3	6.5	8.6	13.4	20.8	3.5	40.0
12	0942N	350	8.6	5.5	7.2	10.6	15.9	3.1	28.9
12	0945W	350	9.4	5.2	7.8	11.0	15.9	3.0	56.6
12	1331N	175	15.0	7.2	11.2	18.2	32.1	3.8	61.1
12	1349W	175	7.8	4.2	5.5	8.9	13.6	2.7	60.1
12	1353N	350	13.5	6.5	9.7	19.3	27.7	3.4	44.6
12	1356W	350	7.8	4.4	6.4	10.3	15.1	2.3	21.0
12	1338N	175	10.4	5.3	7.2	11.7	21.1	2.8	69.9
12	1345W	175	6.9	4.1	5.5	8.2	12.3	2.6	23.8
7	0931N	175	18.8	10.8	15.3	23.3	36.0	6.3	48.0
7	0934W	175	20.6	11.1	15.1	23.0	40.2	5.5	80.3
7	0942N	350	11.0	7.7	10.7	15.1	20.6	4.3	27.8
7	0945W	350	9.2	5.8	7.5	11.0	16.5	3.2	24.3
7	1331N	175	6.2	4.1	5.0	7.4	9.8	2.9	25.7
7	1349W	175	4.8	6.7	9.0	11.8	16.8	3.7	31.7
7	1353N	350	9.8	5.2	7.1	11.9	17.6	3.0	41.6
7	1356N	350	7.9	5.4	6.8	9.9	12.9	3.0	19.4
5	0931N	175	12.0	7.1	9.9	14.3	22.0	4.6	38.3
5	0934W	175	11.7	6.9	9.3	13.3	18.3	4.3	73.3
5	0942N	350	8.5	5.3	6.9	11.0	15.1	3.1	22.1
5	0945W	350	9.2	5.8	7.5	11.0	16.5	3.3	29.3
5	1331N	175	8.4	3.7	6.5	10.0	18.3	0.9	41.8
5	1349W	175	6.2	4.1	5.3	7.4	9.8	2.9	22.8
5	1353N	350	7.2	3.8	5.4	8.7	13.0	2.6	35.4
5	1356N	350	5.1	3.8	4.6	6.0	7.6	2.4	9.7
3	0931N	175	13.4	7.9	10.7	16.3	25.5	4.8	43.7
3	0934W	175	14.0	8.2	10.9	16.1	23.4	5.3	73.4
3	0942N	350	9.3	5.8	7.8	12.2	16.9	3.0	22.3
3	0945W	350	10.0	6.2	8.3	11.5	18.5	3.3	35.7
3	1331N	175	9.3	5.8	7.8	11.4	14.2	3.9	40.1
3	1349N	175	6.2	4.6	5.3	7.4	9.8	2.7	18.2

(Continued)

Table 4 (Concluded)

Time/Dir Elev.			Coherence Lengths (pixels)						
			Mean	Percentiles				Min.	Max.
Ch	(EDT)	ft		25%	50%	75%	90%		
3	1353N	350	7.9	4.4	6.0	9.1	14.9	2.7	39.6
3	1356W	350	2.9	5.0	6.4	9.0	12.9	3.2	27.3
12*	0943N	150	0.73	0.68	0.73	0.79	0.83	0.57	0.96
12*	0944W	150	0.73	0.66	0.73	0.80	0.85	0.57	0.96
12**	1343N	150	8.5	3.7	6.8	12.2	15.9	0.88	41.5
12**	1345W	150	8.4	3.7	6.5	10.0	18.3	0.86	41.8

* June 11, overcast sky, Daedalus D-1261 scanner.

** June 10, overcast sky, Daedalus D-1261 scanner.

change of mean and median coherence length and with a change more like 1.5 than 2.0. At solar noon there is a smaller and less consistent difference than at midmorning. Indeed, for channel 7 at this time, the change of the mean and median coherence lengths is reversed. Scanner system and atmospheric modulation may help moderate altitudinal differences. In any case, the change of the distribution of coherence lengths with altitude does not change in a simple way with the sampling interval.

37. There are no major differences in coherence length distribution with flight direction in the twilight and midmorning data. However, strong directional differences exist in the thermal infrared data taken near solar noon. Here, the mean coherence lengths as well as all the percentile values in Table 4 are considerably larger for the north flights than for the west flights at both altitudes. To determine whether this might be a coincidence, a third flight pair from this time was examined. These flights were flown at 1338 EDT in the north direction and 1345 EDT in the west direction at 175 ft agl. Coherence length distribution parameters are included in Table 4 and confirm the directional difference. The strong solar absorption channels (5 and 3) showing a similar but weaker pattern could be part of an explanation. However, the presence of directional effects near noon but a lack of them at midmorning is very curious. If directional effects are due to shadowing at the scale of trees, then they should have the greatest effects when the sun is low. Possibly this is not observed at the pixel sizes and scan line lengths of these images, but this cannot explain the presence of directional effects near noon. The effects of directional illumination on heat storage,

integrated over the first half of the day, probably contribute. Before the midmorning flights, very little direct irradiance penetrated to the trunk space and ground. As the sun rose, greater amounts of solar energy penetrated deeper into the canopy. (Canopy structure information indicates rapid increases after 0900 EDT.) By solar noon, direct irradiance had been illuminating the subcanopy for several hours, mostly from the south and southeast. A complete explanation of the presence and the changes of directional differences of coherence lengths seems unavailable at this time.

38. There are no dramatic differences observed between spectral bands in the daytime flights. The channel 7 mean and percentile coherence lengths are clearly the largest in the midmorning data. At solar noon, the north-flown thermal infrared images have the largest coherence lengths, but differences between the reflectance bands are inconsistent.

39. One factor contributing to the variability of coherence lengths is the fact that autocorrelation functions have become rather flat when they are near a value of $1/e$. Figure 41 contains plots of the first 20 points in the autocorrelation function (lags 0-19 pixels) from two of the images. The point data are values for the first 50 scan line autocorrelation functions. The lines are least square regression estimates made from the first 20 points of all the autocorrelation functions from an image that did not contain the tower or other instrumentation. The figure indicates that in the vicinity where the autocorrelation is $1/e$ (0.37), a small change in the autocorrelation value can mean a large change in lag. This may be due to scan lines being only a few tree diameters long making the sample too short to be stationary. This conclusion is supported by the fact that autocorrelations do not go to zero until very large lags indicating the presence of low frequency variations. Consequently, while there is much variability in the autocorrelation functions in an image reflected by coherence length distributions, the sensitivity of coherence length to small changes of the autocorrelation function may keep the coherence length from being a very powerful descriptor of autocorrelation in these images.

40. This concludes the analysis of within-image variance and spatial relationships as described by one-dimensional autocorrelation. In the following section, pixel-by-pixel statistical relationships between thermal infrared and reflected energy are developed.

Spectral Relationships

Regression equations

41. The results of the regression of reflectance channel DN values (arbitrary units) on the thermal infrared DN values (in units of 0.1 °C per DN) are summarized in Table 5. As described earlier, all possible combinations of seven independent variables derived from the reflected image data were examined. Using the square of correlation coefficient (r^2) as the criteria for comparing equations, the three variables best correlated individually with the thermal infrared data are listed in Table 5. Along with the r^2 values for the best (highest r^2) equation containing one, four, and all seven independent variables.

Table 5

Summary of the Spectral Regression Relationships

Flight Time (EDT)	Flight Direction	Flight Altitude ft agl	Best			r^2		
			Correlated Variables 1st	2nd	3rd	No. of Variables		
						1	4	7
0931	North	175	DN7	DN7 ²	SUM	0.37	0.38	0.38
0934	West	175	DN7 ²	SUM	DN3	0.52	0.55	0.55
0942	North	350	SUM	DN3	DN7 ²	0.61	0.63	0.67
0945	West	350	SUM	DN7 ²	DN3	0.59	0.62	0.62
1331	North	175	DN5	DN3	DN5 ²	0.21	0.26	0.27
1349	West	175	DN5	DN3	DN5 ²	0.34	0.40	0.41
1353	North	350	DN5	DN3	DN5 ²	0.20	0.26	0.27
1356	West	350	DN5 ²	DN5	DN3	0.08	0.26	0.26

42. The parameter r^2 represents the fraction of the variance in the relationship explained by the equation. Values of r^2 are about twice as high for the midmorning data as the solar noon data. Additionally, equations with one variable do nearly as well as those with four or seven at midmorning, while the change between one and four variables at solar noon is large in relative terms (but small in magnitude). The relationships between the thermal infrared and reflectance pixels appear to be both better and simpler in the morning.

43. The fact that the best individual reflectance variables represent a broader range of the solar spectrum at midmorning than at solar noon is

interesting. The sum and the near-infrared data (given the other variables, channel 3 does not contribute much) perform best in the earlier data while the best individual variables near solar noon are from the absorption channels 3 and 5. Sunlit leaves are generally warmer than shaded leaves, but the assumption that reflected light is proportional to absorbed light is not strictly correct. Additionally, the canopy is not opaque. Woody stems, branches, and the forest floor are partially visible through the tree crowns, and the canopy openings exit in the image. These components may be directly illuminated or shaded. An examination of relationships between changes of reflected light and temperature are of both theoretical and practical interest. However, without detailed analysis of ground information and modeling, the role of these factors cannot be clearly defined.

Three-dimensional spectral histograms

44. Two types of histograms were developed: one for midmorning (0942 EDT) and one near solar noon (1353 EDT). The first type of histogram is a plot of frequency versus channel 5 DN and channel 12 DN and is meant to show the relationship between solar absorption and temperature. Two views of each of these histograms are given in Figures 42 and 43. Channel 5 has the greatest solar absorptance of the reflectance channels. The other type of histogram uses the near-infrared to red ratio (often used as an index of green vegetation) and the thermal infrared. Hopefully, the DN7/DN5 value would help distinguish between the green canopy and other forest components. Two views of each histogram are given in Figures 44 and 45.

45. The first type of histogram (DN5 versus DN12) at midmorning data shows a fairly smooth distribution of frequencies moderately skewed with a peak toward the low values of each channel. At solar noon the distribution is not as smooth and, on the channel 5 axis, is somewhat skewed so that the peak is toward the high values. The thermal infrared at solar noon has no skew if a small group of points with very high channel 12 DN's and moderate channel 5 DN's are considered to be separate population. These pixels (channel 12 DN of 230 or more, channel 5 DN in the neighborhood of 100) are associated with sunlit forest openings and, therefore, can be considered as a separate scene component. (Ground measurements indicated that dry dead leaves in the openings could have a radiant temperature on the order of 60 °C while the green canopy leaves had a temperature near 20 °C. These openings normally consisted of some herbaceous plants and tree seedlings along with the dry leaves and some shadows which moderated the average pixel temperatures from that of the

dry leaves. Sunlit openings were, by far, the warmest parts of the channel 12 images and may be misconstrued as targets.) The lack of skew in the thermal infrared contrasts with observations of desert terrain (Ben-Yosef, Wilner, and Abitbol 1986) where strong skewness was observed near noon at comparable spatial resolution but at very high nadir angles. (Twilight thermal infrared scanner data were also unskewed.) Unfortunately, sunlit and shaded parts of the forest canopy cannot be distinguished on the basis of these histograms.

46. Histograms of the DN7/DN5 ratio and channel 12 DNs are more complex. Frequencies are skewed along the ratio axis so that there is a peak toward low values at midmorning and high ratios at solar noon. This implies that it is relatively greener at solar noon than at midmorning--a condition which is not true. Actually, the ratio depends on sun angle (different spectral directional reflectance) as well as the relative near-infrared and red irradiance which changes with time, shadowing, and depth in the canopy. It may not be a robust index under the target-viewing conditions of these data which fail to average or normalize these effects. There does seem to be a relationship between the variables at 0942 EDT, but it appears much weaker at solar noon. None of the histograms provide much information useful for improving the quantification of relationships between the thermal infrared images and images of reflected energy.

PART V: CONCLUSIONS AND RECOMMENDATIONS

Variance and Autocorrelation

47. The standard deviation of the thermal infrared imagery increases with time through the study period. There is some evidence that this change is not symmetrical around solar noon (Balick et al. 1987), and there are suggestions in these data that the daily energy budget differences of different forest components, particularly heat storage, integrated over time noticeably affect the thermal infrared data. With only three data points in time over only one half a diurnal cycle, little can be said about how image variance changes over shorter periods of time. In general, the role of heat storage and varying heating rates of forest components is of great importance to thermal modeling of forests and needs to be investigated more thoroughly. Of necessity, this would include time-intensive airborne data over a day and detailed ground measurements and modeling of heat-storing forest components that would render an understanding of the physical processes involved. Also, a rather complete description of the forest canopy structure would be needed.

48. There is no indication that image variance changes between the two flight altitudes in any channel. This is somewhat of a surprise in that the areas sampled in individual pixels differ by a factor of 4 and that the autocorrelation functions do vary with altitude. However, the autocorrelation functions do not change as much as would be expected using simple considerations. System and atmospheric modulations were not taken into account. The altitude difference is not really very large, and sampling effects must be observed at some point. The issue needs clarification and generalization and is a topic amenable to analysis in spatial statistics.

49. One-dimensional autocorrelation functions vary greatly throughout individual images. Two-dimensional autocorrelation functions would be a more powerful descriptor of spatial relationships but cannot be used here because of the lack of spatial fidelity in the flight direction. Forest openings, sunlit or shaded, can induce large changes of the autocorrelation function. They often appear similar to changes sometimes caused by the tower; thus, they may be potential false targets in frequency space. This is especially true for the sunlit gaps in the thermal infrared which are most common at high solar elevation angles. Since they are the hottest parts of the forest scene, they also may be false targets in image space.

50. The coherence length of the autocorrelation function was used as a descriptive parameter of the one-dimensional autocorrelation functions. These were seen to vary greatly within images--often changing over an order of magnitude. Using coherence length as a parameter for image texture model risks great oversimplification of the spatial variations found in these images. Although a single value of coherence length did not provide a robust description of spatial variations within images, frequency distributions of this parameter within images showed detectable and repeatable differences between images. Directional differences, especially strong in the thermal infrared, were observed near solar noon when the flight directions were parallel and perpendicular to the azimuth to the sun. These differences were not observed in the midmorning, but the flight directions then would minimize this effect. Future data acquisition should be considered where flight lines rotate with the solar azimuth. Coherence length distributions changed considerably less than in direct proportion to the sampling interval or pixel size. To a large extent, this may be due to scanner system modulations (which have not yet been characterized for operation in the 1.25-milliradian IFOV mode). However, spatial statistics can support the generalization of the effects of sampling changes on autocorrelation (and variance) in a quantitative way. Mean and median coherence lengths tend to be highest in the near-infrared (channel 7) and in the midmorning. However, excluding the twilight thermal data, mean and median coherence lengths do not vary widely from band to band. A crosscorrelation analysis might provide additional and interesting information on spatial-spectral relationships. Finally, the shape of the autocorrelation function in these data contributes to the variability of the coherence length. Since this depends on the spatial scale at which variations of DN's occur, how they are observed, and sample size, this effect is generally important in measuring or modeling parameters for scene modeling applications.

51. The high spatial resolution of the data is not directly applicable to most remote sensing or tactical applications, nor is it tractable for physical models. One motivation for obtaining these data was to take advantage of an opportunity to observe forests in greater detail than models can simulate; this would ensure that small-scale effects were properly parameterized or otherwise included in the models. Another is simply to get a look at the detail averaged to obtain lower resolution imagery and thereby gain greater insights for understanding those data. Unfortunately, in doing so we are barely able to see the trees for the leaves. Even at 350 ft agl, a scan line

is only three or four trees long. The shape of the autocorrelation functions--the slow decrease of correlation at a fairly high value after the initial drop--indicates that there is low-frequency variation along scan lines. However, the function is being dominated by the high-frequency variations. Coherence lengths and the interesting portions of the autocorrelation functions are over distances of less than a meter, which are less than the scale of variations associated with trees or even major branches. While it would be best to obtain future data over a wider range of altitudes, reanalysis of these data after low pass filtering might show variations associated with larger scales of forest structure.

52. The spatial resolutions are about those of airborne laser remote sensing and designating systems. Intuitively, the image variability information would be relevant to laser return variability. Channels 3 and 5 more closely represent single-scattering beam reflectance processes and may, therefore, be most appropriate even for lasers operating in the near-infrared. Although reflectance measurements at this scale are not a sufficient approximation of laser backscattering, they at least describe the background in which the laser signal must be detected during the day. Greater consideration should be given to the relationships between solar and laser directional reflectance variability.

53. It is clear that the parameters used for texture modeling in scene simulation software vary with solar position and possibly other time or environment varying factors. Extrapolation of parameter values obtained from images must be done with care and knowledge of the environmental influences on them. Sensor system and atmospheric effects must also be considered in defining texture model parameters.

Spectral Relationships

54. The statistical correlation between the reflected energy measurements and the thermal infrared is mediocre at midmorning and poor at solar noon. It is possible that time-dependent heat storage effects over the morning and time-varying stomatal function (transpiration) decrease relationships between instantaneous direct irradiance and temperature in the canopy. It is also possible that greater penetration of the direct irradiance to the tree stems, understory, and forest floor complicated both the images of reflected and thermal energy (within-image variance increased and coherence lengths

tended to decrease) and the relationships between them. Additionally, changes in atmospheric conditions may have had effects particularly in changing the irradiance in the shadowed portions of the image. The dramatic shift of skew of the data with DN7/DN5 ratios in the histograms indicates that instantaneous solar energy transfers within the canopy change between observation periods. (Thermal responses are not involved in this change.) These relationships are important from both the theoretical and practical perspectives and need to be better understood. Airborne and ground data taken through the entire day would be needed to define the physical and physiological processes and their relative importance to changing the relationships between reflected and emitted energy in forests.

55. A rather superficial statistical examination of the data was performed to try to separate the effects of shadowing and of pixel content (green leaves versus other materials) without much success. It is possible to perform more detailed and intensive analyses. Image transformations such as ratio can be performed to better segment the original image into a small number of classes. Such classes can also be based on image interpretation of shadowing and scene contents or by machine pattern recognition. Analysis of variance or regression analysis would be done on each class separately, and the results from both times compared to determine how relationships change over time. Such analyses would be useful in designing experimental plans for more intensive measurement programs.

REFERENCES

- Ahuja, N., and Schachter, B. J. 1983. Pattern Models. John Wiley and Sons, Inc., New York.
- Baldocchi, D. D., Hutchison, B. A., Matt, D. R., and McMillen, R. T. 1984. "Seasonal Variations in the Radiation Regime within an Oak-hickory Forest," Agric. and Forest Meteorology, Vol 33, pp 177-191.
- _____. 1985. "Canopy Radiative Transfer Models for Spherical and Known Inclination Leaf Angle Distributions: A Test in an Oak-hickory Forest," J. Appl. Ecology, Vol 22, pp 539-555.
- _____. 1986. "Seasonal Variation in the Statistics of Photosynthetically Active Radiation Penetration in an Oak-hickory Forest," Agric. and Forest Meteorology, Vol 36, pp 343-361.
- Balick, L. K., Hutchison, B. A., Smith, J. A., and McGuire, M. J. 1987. "Directional Thermal Infrared Existence Distributions of a Deciduous Forest in Summer," IEEE Trans. Geosci. Remote Sensing, Vol GE-25, No. 3, pp 410-412.
- Ben-Yosef, N., Rajat, B., and Fiegan, G. 1983. "Simulation of IR Images of Natural Backgrounds," Applied Optics, Vol 22, No. 1, pp 109-193.
- Ben-Yosef, N., Wilner, K., and Abitol, M. 1986. "Radiance Statistics vs Ground Resolution in Infrared Images of Natural Terrain," Applied Optics, Vol 25, No. 16, pp 2648-2649.
- Ben-Yosef, N., Wilner, K., Simhony, S., and Abitol, M. 1986. "Correlation Length of Natural Terrain Infrared Images: Daily Variation," Applied Optics, Vol 25, No. 6, pp 866-868.
- Botkin, E., Krassner, J., Wise, K. S., Grawronski, G., and D'Argenio, C. S. 1981. "Infrared Modeling and Analysis - Environmental Model/Scene Generator," Prepared by the Grumman Aerospace Corporation and Analytics, Inc. for the U.S. Air Force Armament Div. AF Armament Lab., Eglin Air Force Base, FL.
- Faugeras, O. D. 1980. "Autoregressive Modeling with Conditional Expectations for Texture Synthesis," IEEE 5th International Conference on Pattern Recognition 2, No. CH1499-3/80/0000-0792, pp 792-794.
- Finlay, W. M., Weathersby, M. R., and Gaby, J. E. 1983. "Computer Generated 3-D Infrared Background Imagery Model," Report A-3425, Engineering Experiment Station, Georgia Institute of Technology, Atlanta, GA.
- Haralick, R. M. 1979. "Statistical Structural Approaches to Texture," Proceedings of the IEEE, Vol 67, No. 5, pp 705-721.
- Hutchison, B. A., and Matt, D. R. 1977. "The Distribution of Solar Radiation within a Deciduous Forest," Ecological Monographs, Vol 47, No. 2, pp 186-207.
- Hutchison, B. A., Matt, D. R., McMillan, R. T., Gross, L. J., Tajchman, S. J., and Norman, J. M. 1986. "The Architecture of a Deciduous Forest in Eastern Tennessee, USA," J. Ecology, Vol 74, pp 635-646.
- Kimes, D. S., and Kirchner, J. A. 1982. "Radiative Transfer Model for a Heterogeneous 3-D Scene," Applied Optics, Vol 21, No. 22, p 4119.
- Li, X., and Strahler, A. H. 1986. "Geometric-optical Bidirectional Reflectance Modeling of a Coniferous Forest Canopy," IEEE Trans. Geosci. Remote Sensing, Vol GE-24, pp 906-919.

Loefer, G. R., Schneider, D. E., Finlay, W. M., and Weathersby, M. R. 1983. "An Infrared Background Clutter Model Using 3-D Computer Graphics," IEEE CG and A, (March/April), pp 55-66.

Otterman, J. 1984. "Albedo of a Forest Modeled as a Plane with Dense Protrusions," J. Climate Appl. Meteor., Vol 22, pp 297-307.

Rosenfeld, A. 1981. Image Modeling. Academic Press. New York.

SAS Institute. 1987. SAS User's Guide: Basics. Version 5 Edition, SAS Institute, Inc., Cary, NC.

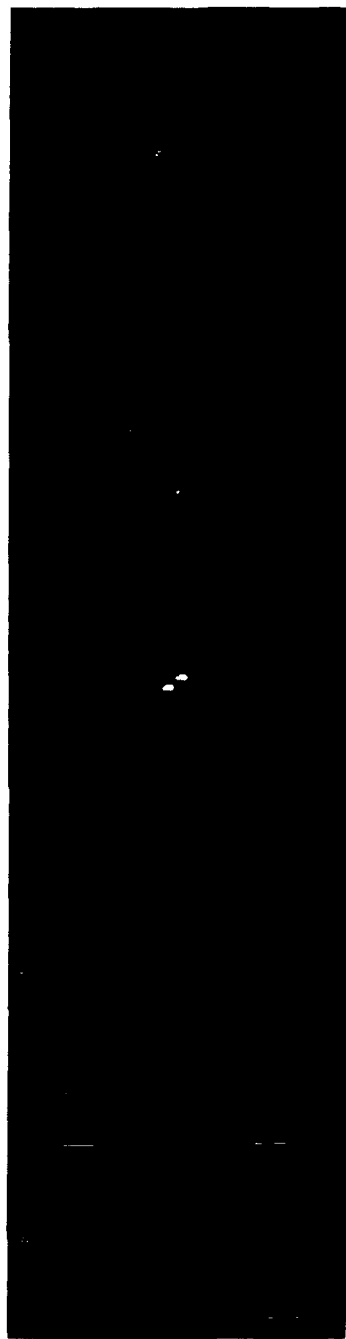
Smith, J. A. 1983. "Matter-energy Interaction in the Optical Region," Manual of Remote Sensing, 2d ed., R. N. Colwell, Ed., Amer. Society of Photogrammetry, pp 61-113.

Smith, J. A., Ranson, K. J., Nguyen, D., Balick, L. K., Link, L. E., Fritschen, L., and Hutchison, B. A. 1981a. "Thermal Vegetation Canopy Model Studies," Remote Sensing of Environ., Vol 11, pp 311-326.

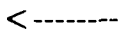
Smith, J. A., Ranson, K. J., Nguyen, D., and Link, L. E. 1981b. "Thermal Vegetation Canopy Model Studies," Technical Report EL-81-6, prepared by Colorado State University in collaboration with the Environmental Laboratory, U.S. Army Engineer Waterways Experiment Station, Vicksburg, MS.

Strahler, A. H., and Li, X. 1981. "An Invertible Coniferous Forest Canopy Reflectance Model," in Proc. 15th Int. Symp. Remote Sensing of Environ. pp 1237-1244.

Strahler, A. H., Woodcock, C. E., and Smith, J. A. 1986. "On the Nature of Models in Remote Sensing," Remote Sensing of Environ., Vol 20, pp 121-139.



0944 - WEST
Ch 12 - at 150 ft



1345 - WEST
Ch 12 - at 150 ft

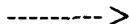
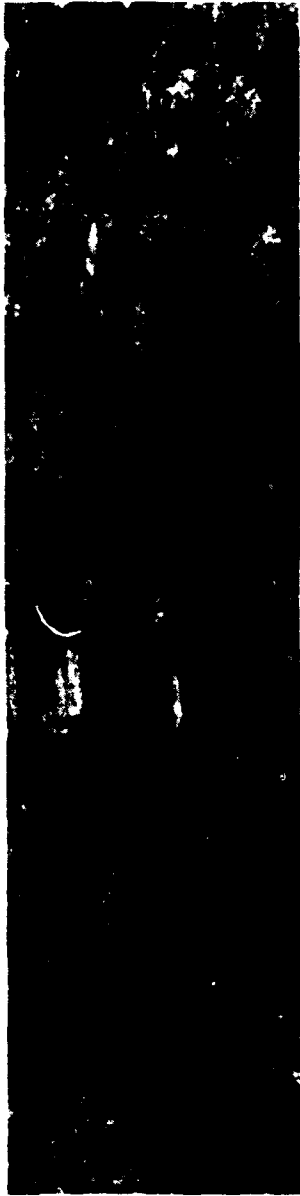


Figure 1. Channel 12 thermal infrared images of the canopy under overcast conditions using a Daedalus D-1261 scanner. The image on the left was obtained at midmorning on 11 June 1986, and the image on the right was obtained on June 10 at solar noon at an altitude of 150 ft agl in the west direction. The images are 2,048 by 512 pixel images used in the analysis but subsampled by a factor of 4 in each direction

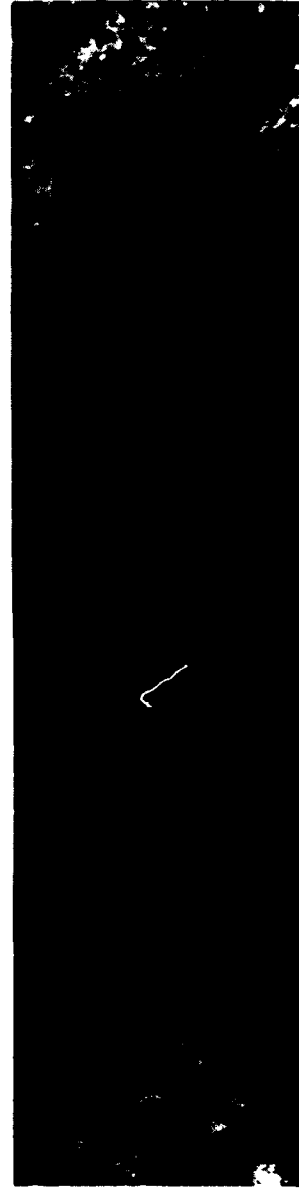
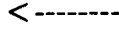


0604 - WEST
Ch 12 - at 350 ft

Figure 2. Predawn twilight thermal infrared image (channel 12) of the canopy. This image was obtained under clear skies on 16 June 1986 using a Daedalus D-1268 multispectral scanner at an altitude of 350 ft agl flown in the west direction. The image is 2,048 by 512 pixel images used in the analysis but subsampled by a factor of 4 in each direction for display



0945 - WEST
Ch 12 - at 350 ft



934 - WEST
Ch 12 - at 175 ft

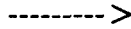
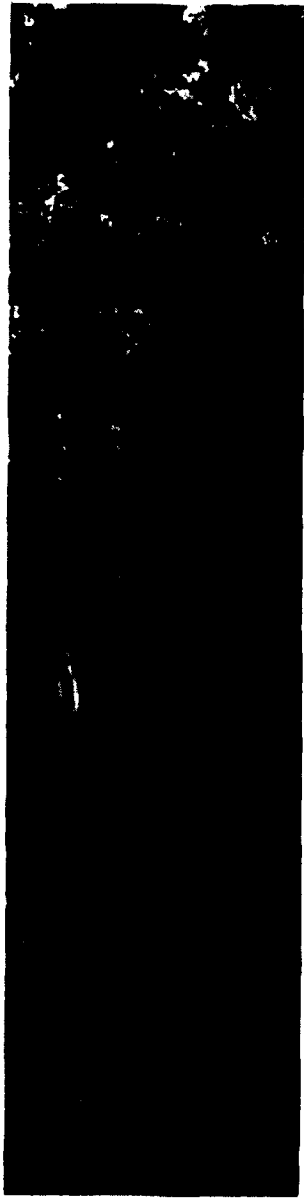
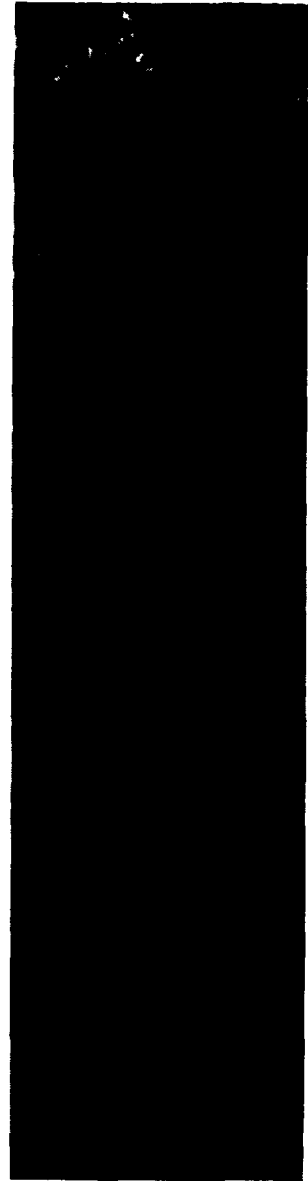


Figure 3. Conditions as in Figure 2 except midmorning data at altitudes of 350 ft agl (left) and 175 ft agl (right)



0945 - WEST
Ch 7 - at 350 ft

<-----



0934 - WEST
Ch 7 - at 175 ft

----->

Figure 4. Conditions as in Figure 3 except data are from channel 7



1353 - NORTH
Ch 12 - at 350 ft



1356 - WEST
Ch 12 - at 350 ft



Figure 5. Conditions as in Figure 3 except data are taken near solar noon in the north (left) and west direction (right) at an altitude of 350 ft agl



1353 - NORTH
Ch 7 - at 350 ft



1356 - WEST
Ch 7 - at 175 ft

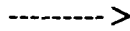
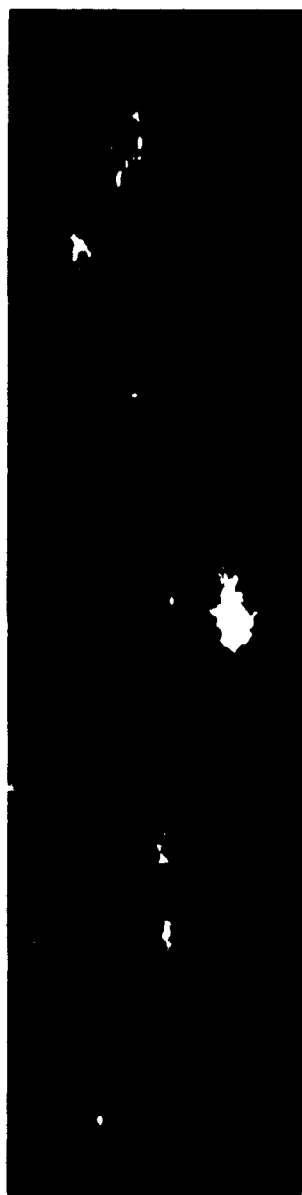
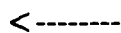


Figure 6. Conditions as in Figure 5 except data from channel 7



1353 - NORTH
Ch 5 - at 350 ft



1356 - WEST
Ch 5 - at 350 ft

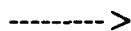


Figure 7. Conditions as in Figure 5 except data are from channel 5

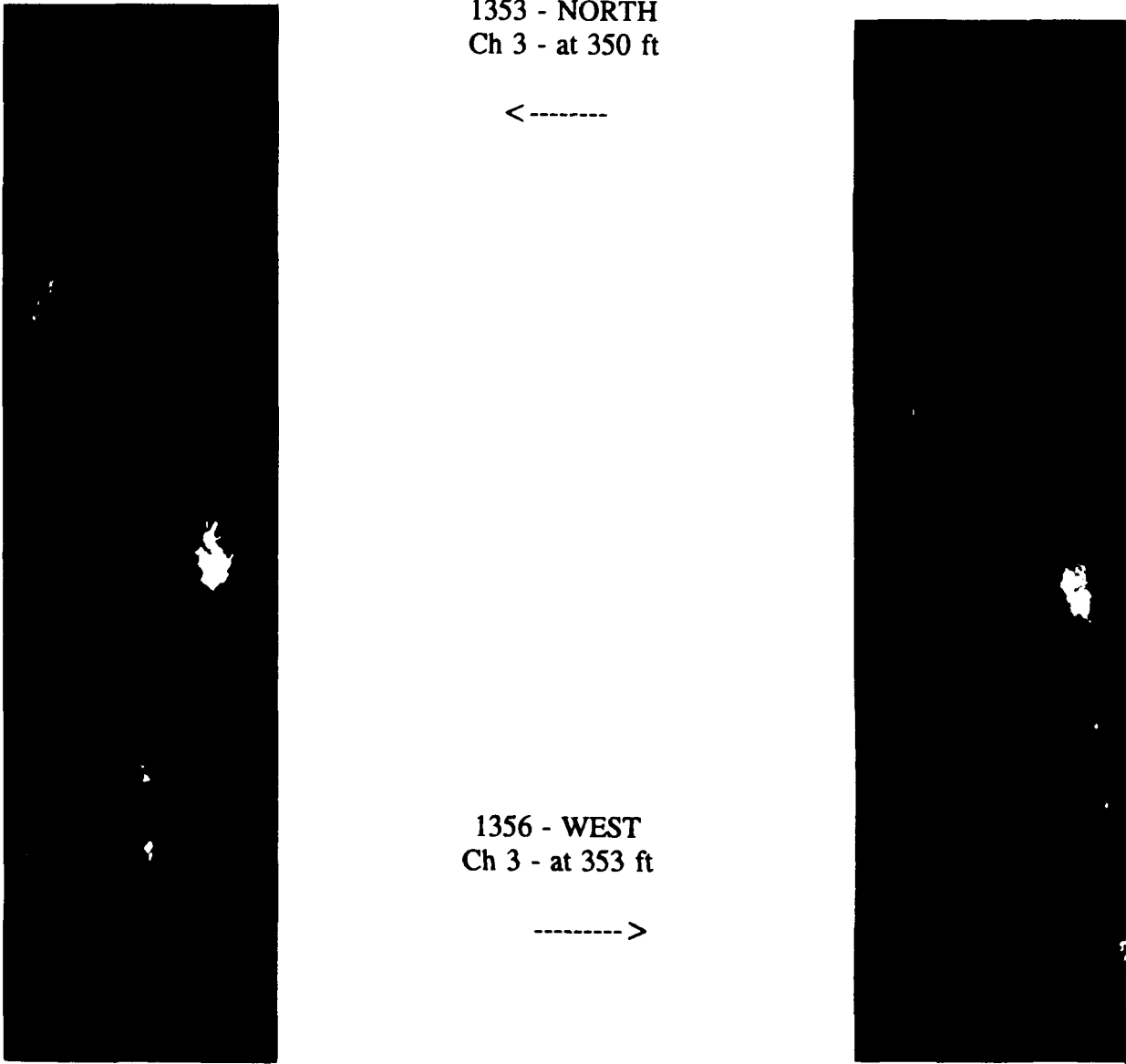


Figure 8. Conditions as in Figure 5 except data are from channel 3

1345 - WEST
Ch 12 - at 150 ft



Figure 9. A 512 by 512 (full resolution) subsection of the channel 12 thermal infrared image on the right of Figure 1. The tower is at the top of the subsection

0604 - WEST
Ch 12 - at 350 ft

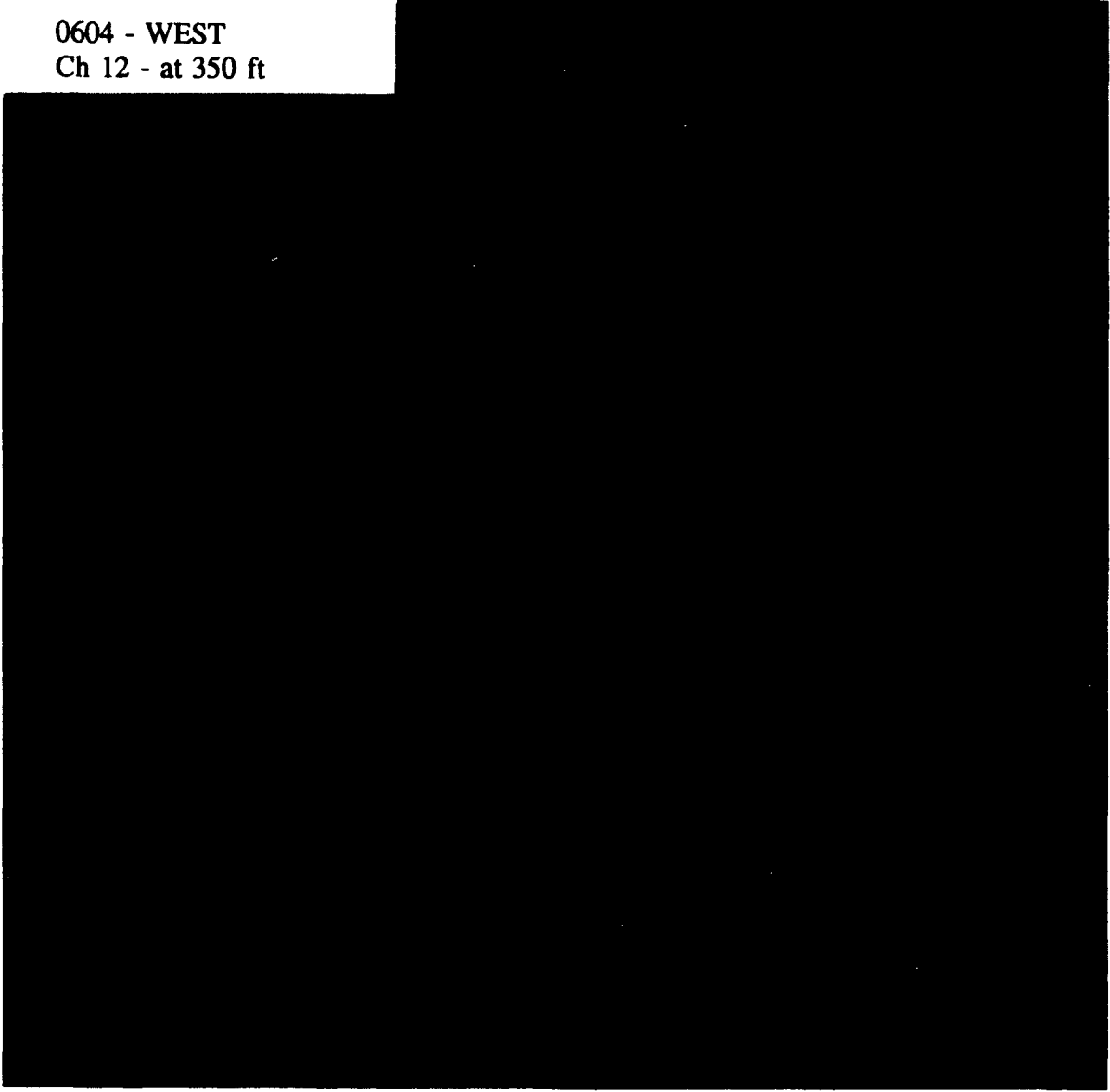


Figure 10. Conditions as in Figure 9 except corresponds to data in
Figure 2

0931 - NORTH
Ch 12 - at 175 ft

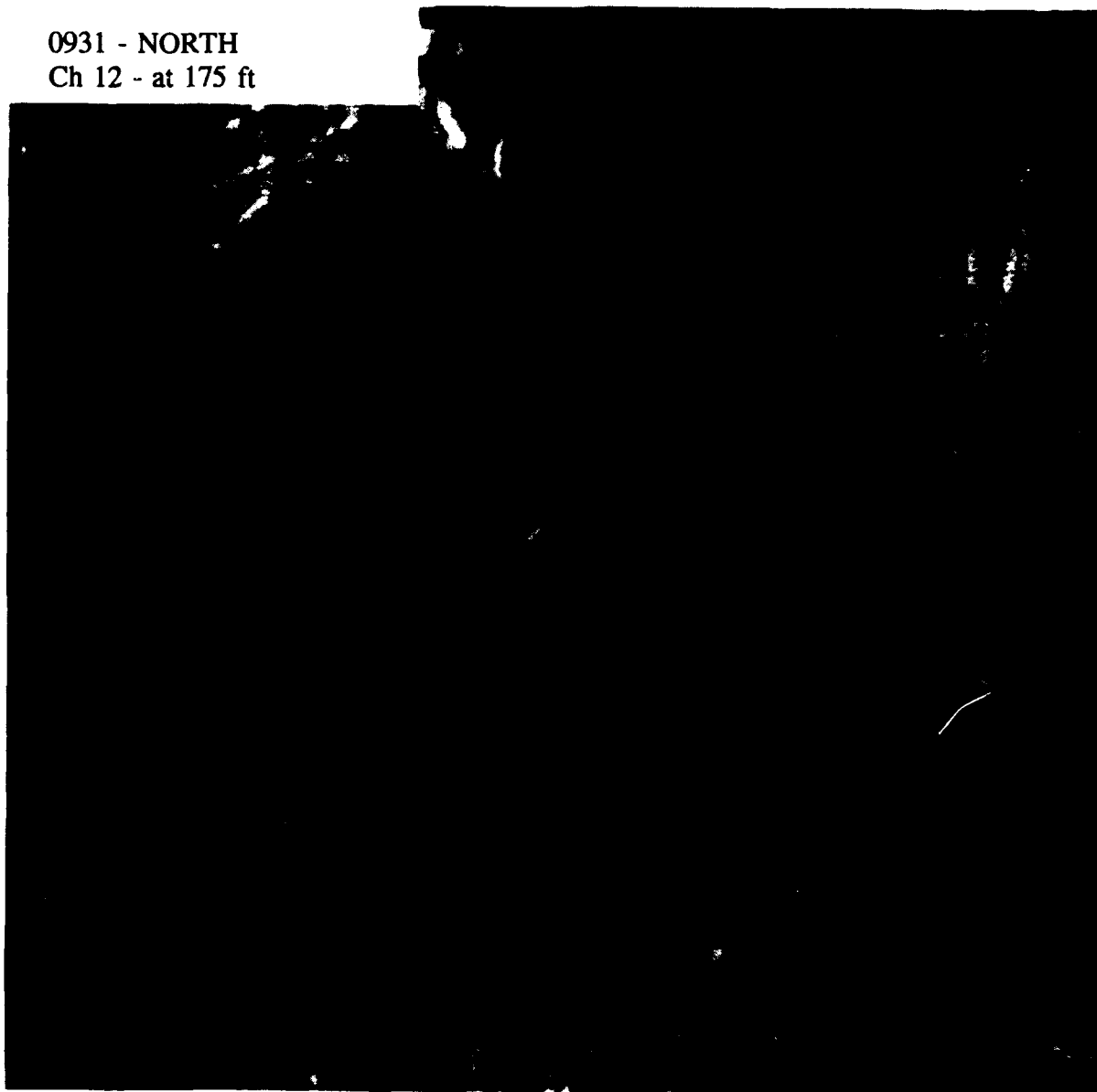


Figure 11. Conditions as in Figure 9 except from the midmorning north flight at 175 ft agl

0934 - WEST
Ch 7 - at 175 ft

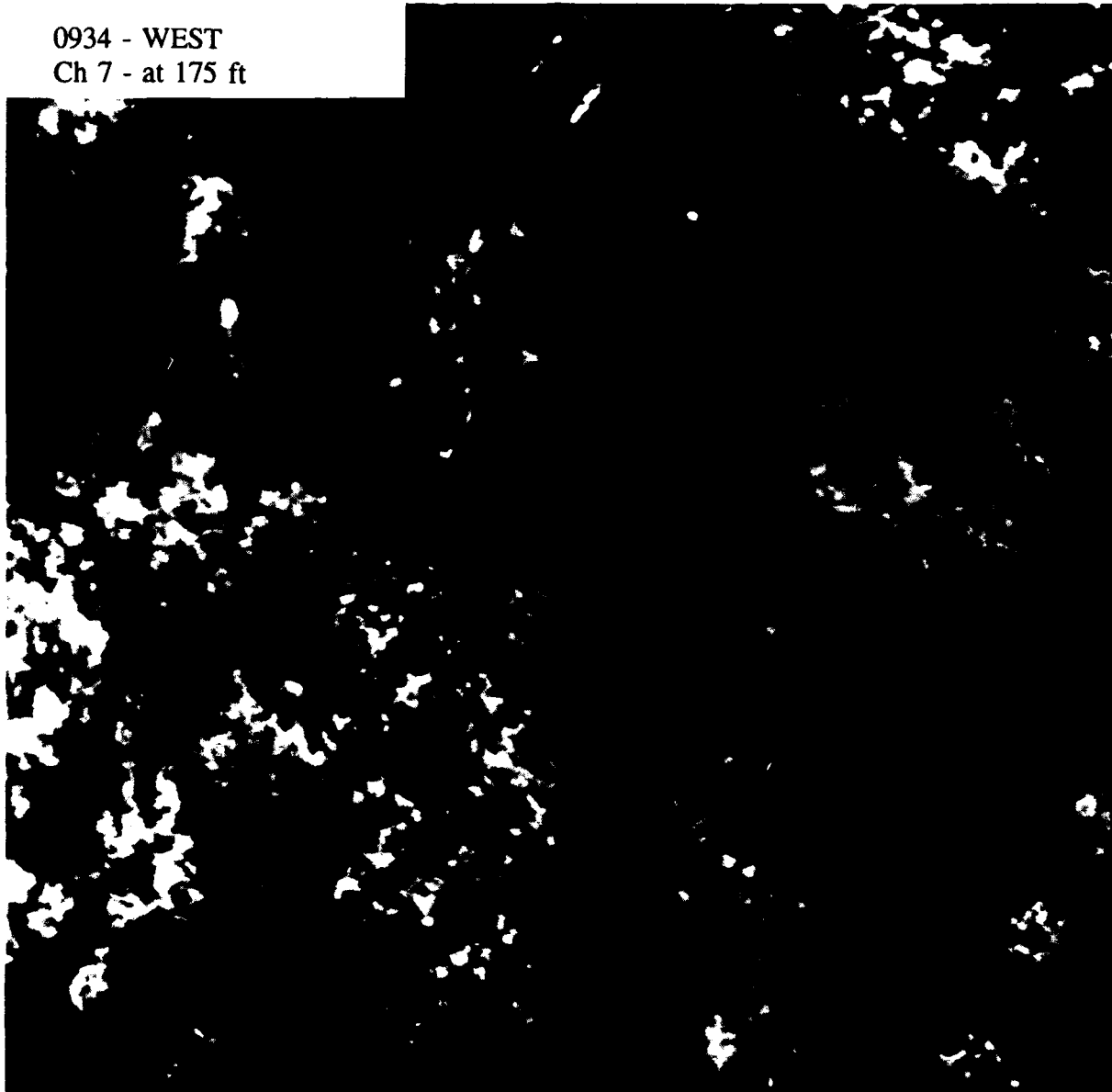


Figure 12. Conditions as in Figure 11 except the data are from channel 7

0934 - WEST
Ch 5 - at 175 ft

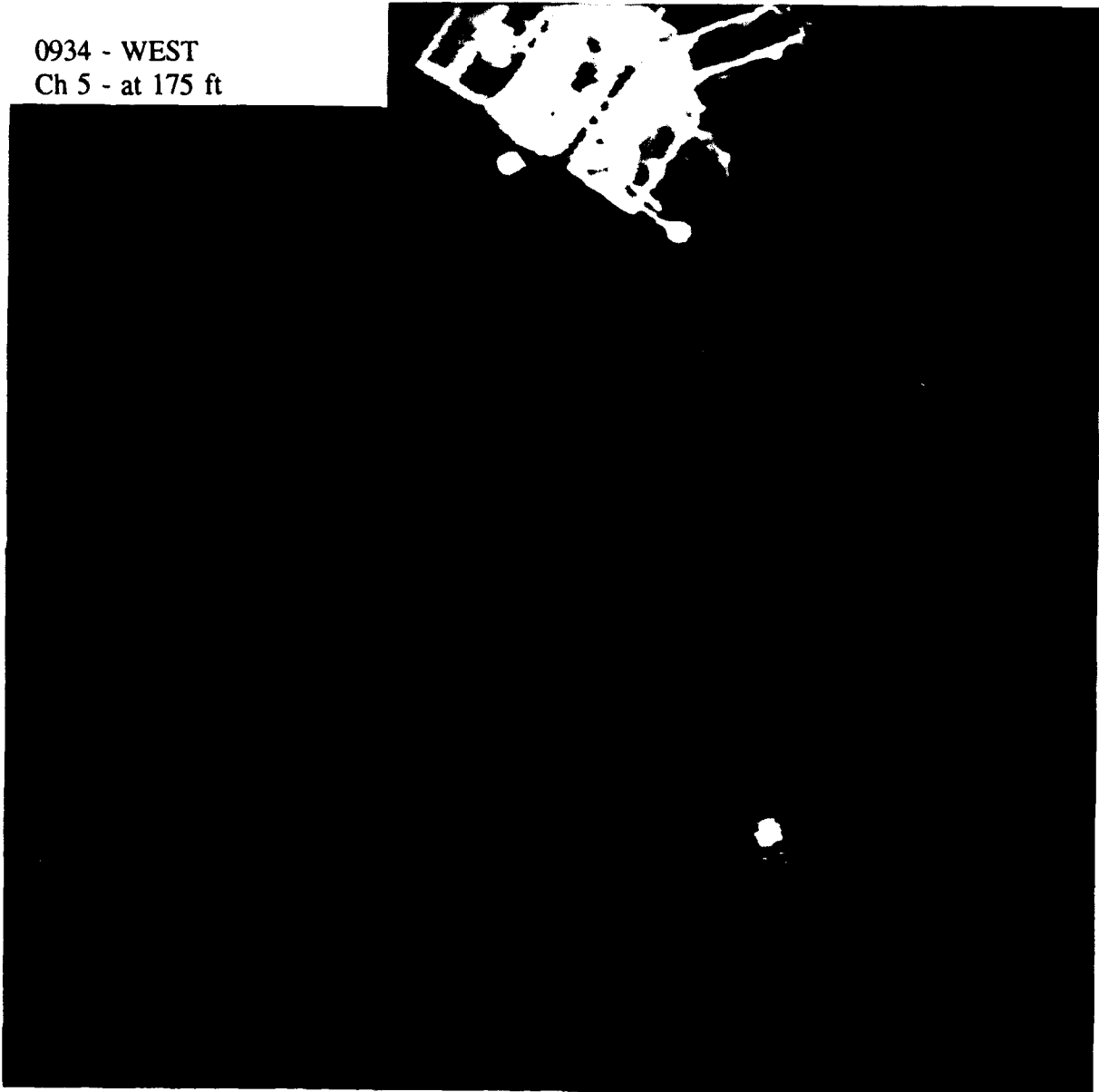


Figure 13. Conditions as in Figure 11 except the data are from channel 5

1356 - WEST
Ch 12 - at 350 ft

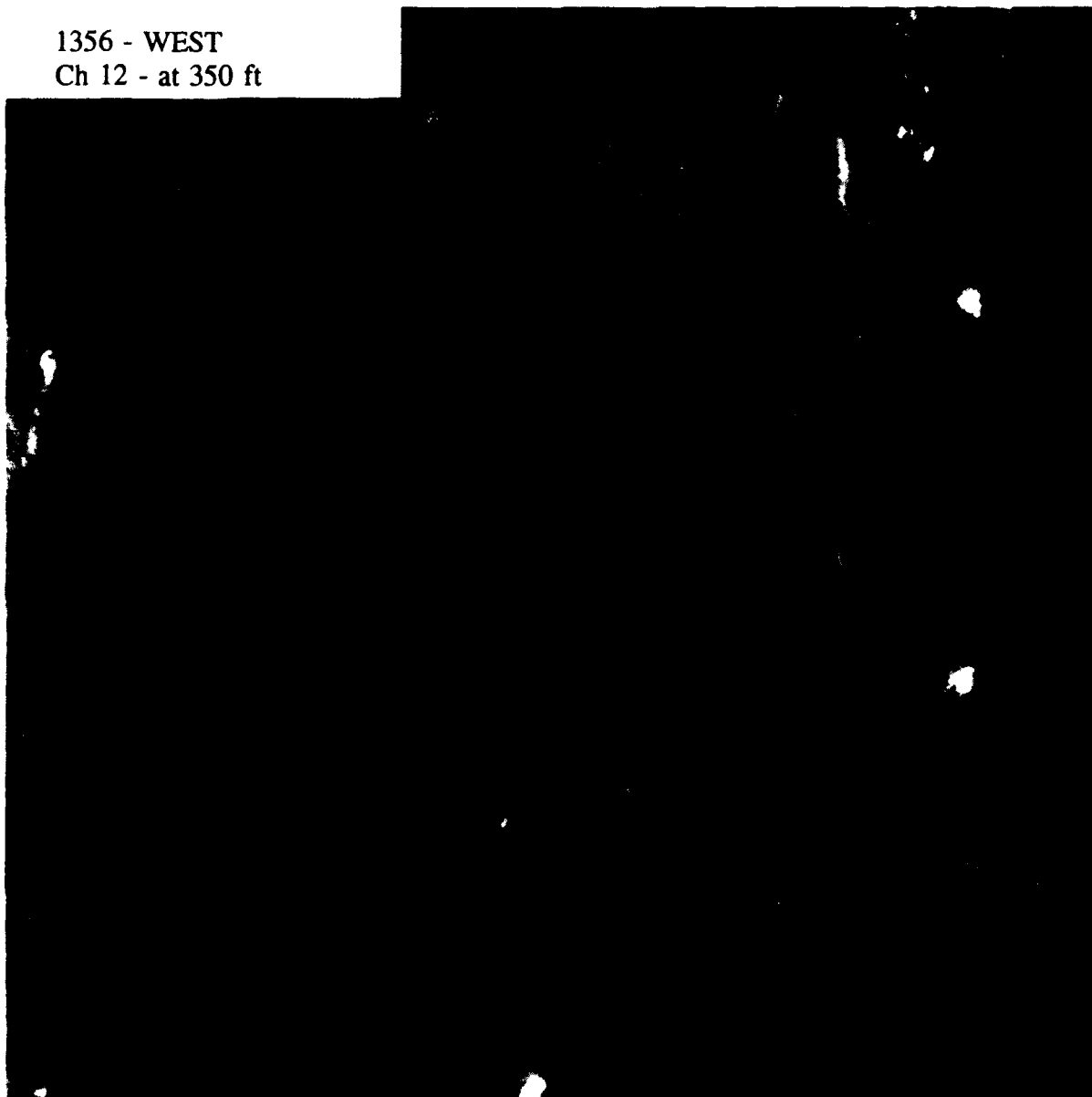


Figure 14. Conditions as in Figure 11 except the data are taken at
350 ft agl near solar noon

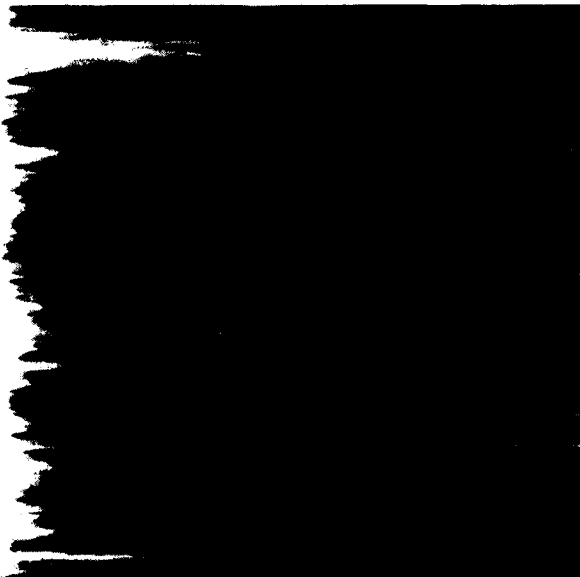
1353 - NORTH
Ch 12 - at 350 ft



Figure 15. Conditions as in Figure 14 except data are taken in the north flight direction



0604 - WEST
Ch 12 - at 350 ft



0945 - WEST
Ch 12 - at 350 ft

Figure 16. Pictorial presentation of one-dimensional autocorrelation functions. Distance (lag) increases from 0 at the left edge to 256 at the right edge. Each line (row) is the autocorrelation function for every eighth line of image data. Brightness is proportional to the value of autocorrelation. Autocorrelations are for the predawn twilight (top) and the midmorning (bottom) thermal infrared images flown in the west direction at 350 ft agl



0945 - WEST
Ch 7 - at 350 ft

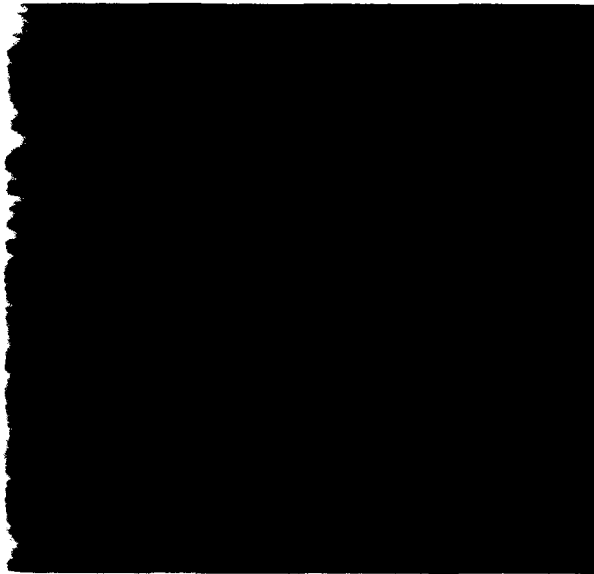


0945 - WEST
Ch 5 - at 350 ft

Figure 17. Conditions as in Figure 16 except data are from channels 7 (top) and 5 (bottom)

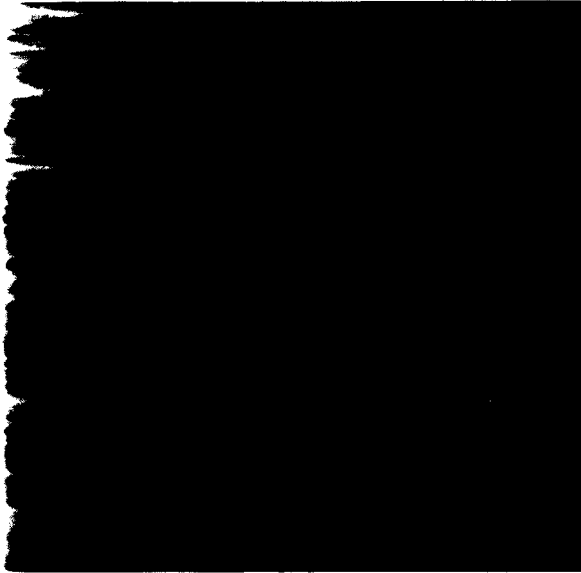


1353 - NORTH
Ch 12 - at 350 ft

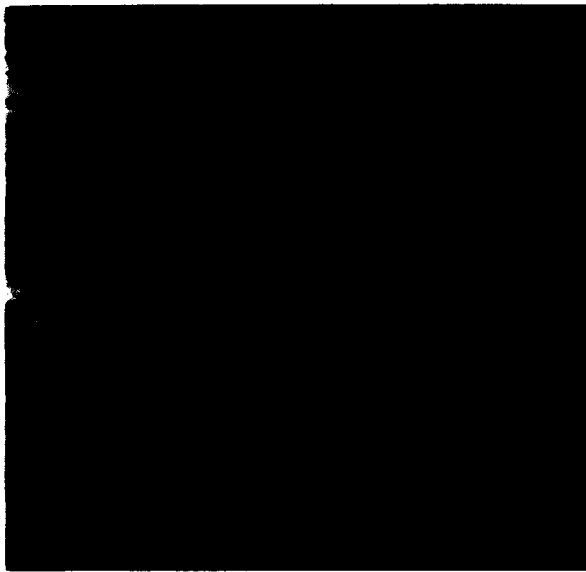


1356 - WEST
Ch 12 - at 350 ft

Figure 18. Conditions as in Figure 16 except the data are from the north (top) and west (bottom) flights at 350 ft agl near solar noon



1353 - NORTH
Ch 7 - at 350 ft



1353 - NORTH
Ch 5 - at 350 ft

Figure 19. Conditions as in the top of Figure 18 except the data are from channels 7 (top) and 5 (bottom)



1356 - WEST
Ch 7 - at 350 ft



1356 - WEST
Ch 5 - at 350 ft

Figure 20. Conditions as in the bottom of Figure 18 except the data are from channel 7 (top) and channel 5



0934 - WEST
Ch 12 - at 175 ft



0931 - NORTH
Ch 12 - at 175 ft

Figure 21. Conditions as in Figure 18 except flights are at 175 ft agl

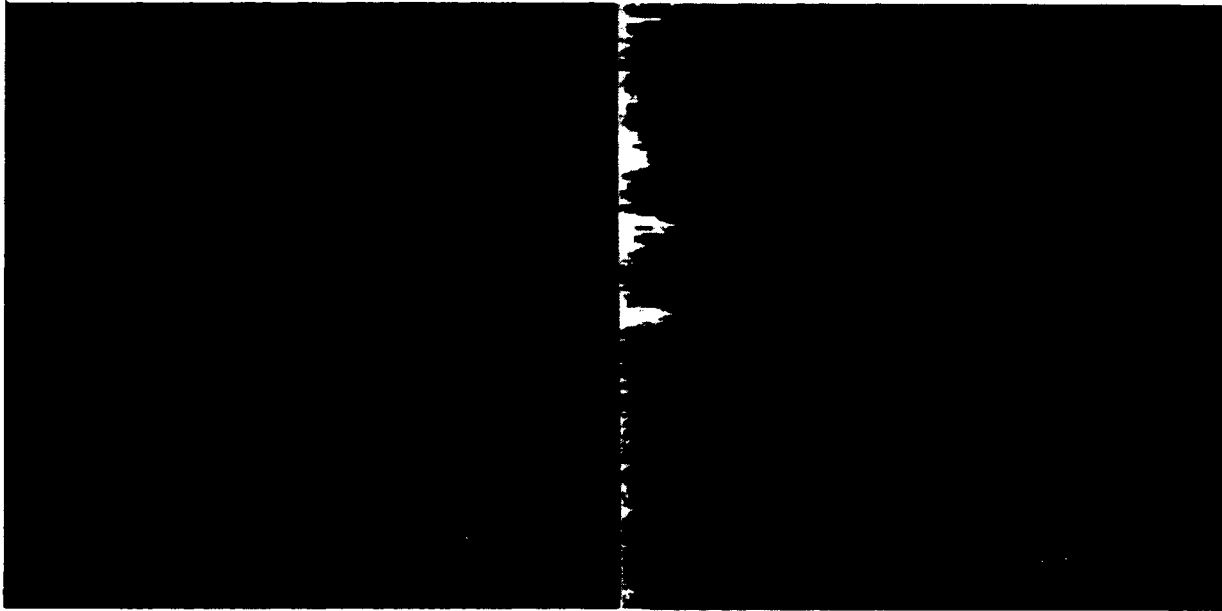


0931 - NORTH
Ch 7 - at 175 ft



0931 - NORTH
Ch 5 - at 350 ft

Figure 22. Conditions as in the bottom of Figure 21 except the data are from channels 7 (top) and 5 (bottom)

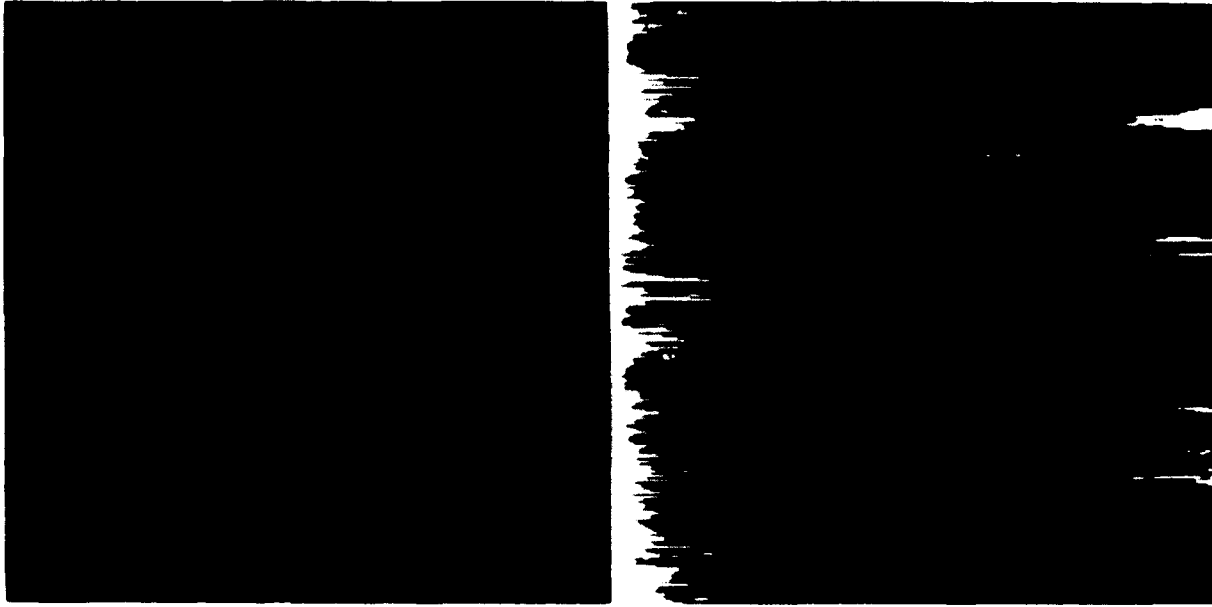


Scanner Data

Auto-Correlation

0604 - WEST - Ch 12 - at 350 ft

Figure 23. Scanner data and corresponding one-dimensional autocorrelations. Every eighth line of the 2,048 by 512 images is given on the left with the corresponding autocorrelation on the right. Autocorrelations are presented the same way as Figures 20-27 except values larger than $1/e$ (0.37) in the equivalent real-value images are mapped to light grey 1.0. The distance from the left edge of the autocorrelation length to the first right edge of the mapped pixels is proportional to the coherence length. Data are from thermal infrared channel of the predawn twilight flight at 350 ft agl in the west direction



Scanner Data

Auto-Correlation

0931 - NORTH - Ch 12 - at 175 ft

Figure 24. Conditions as in Figure 23 except data are from the midmorning flight in the north direction at 175 ft agl

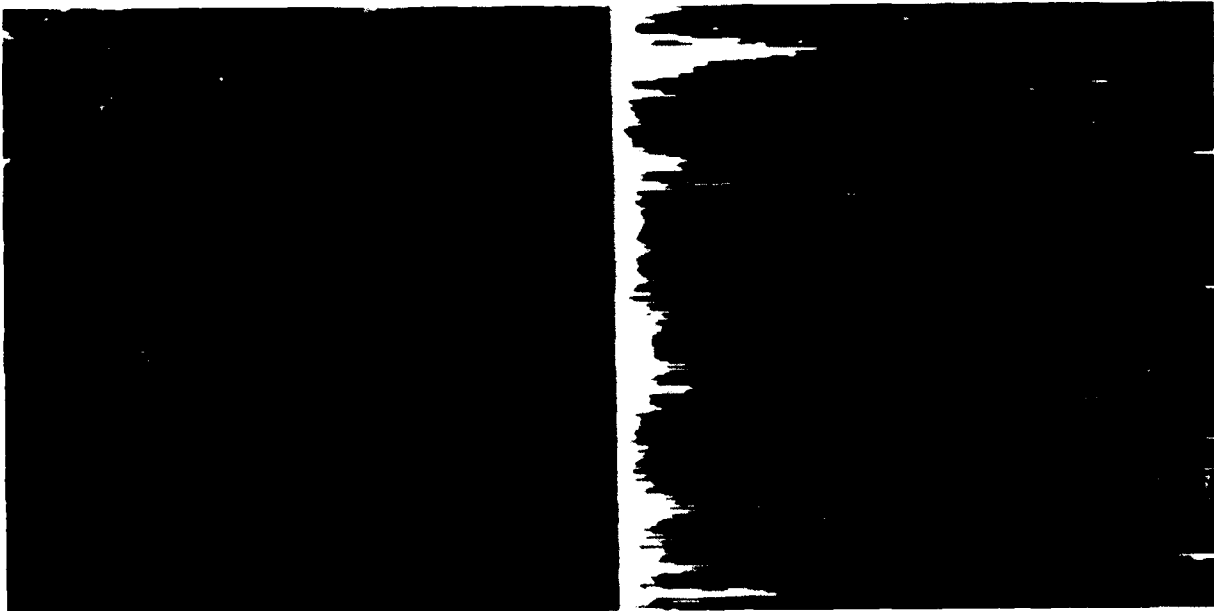


Scanner Data

Auto-Correlation

0945 - WEST - Ch 12 - at 350 ft

Figure 25. Conditions as in Figure 24 except data are from the west flight direction at 350 ft agl

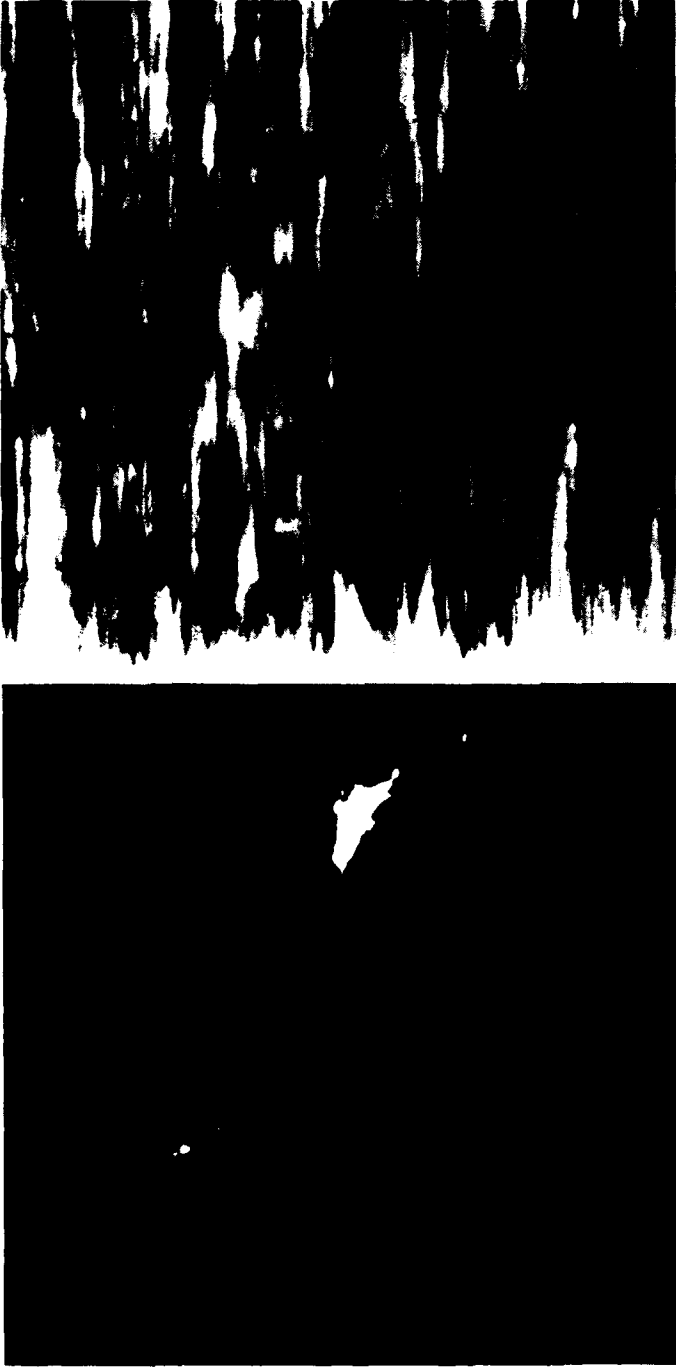


Scanner Data

Auto-Correlation

0945 - WEST - Ch 7 - at 350 ft

Figure 26. Conditions as in Figure 25 except data are from channel 7

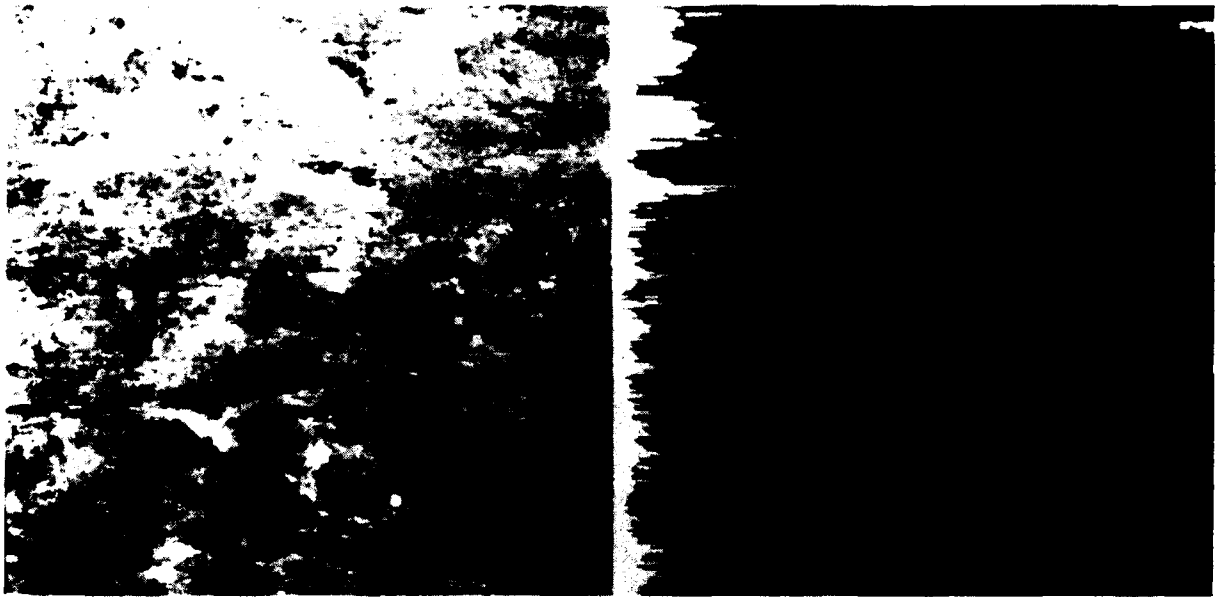


Scanner Data

Auto-Correlation

0945 - WEST - Ch 5 - at 350 ft

Figure 27. Conditions as in Figure 25 except data are from channel 5



Scanner Data

Auto-Correlation

1353 - NORTH - Ch 12 - at 350 ft

Figure 28. Conditions as in Figure 25 except data are from the north flight at 350 ft agl near solar noon

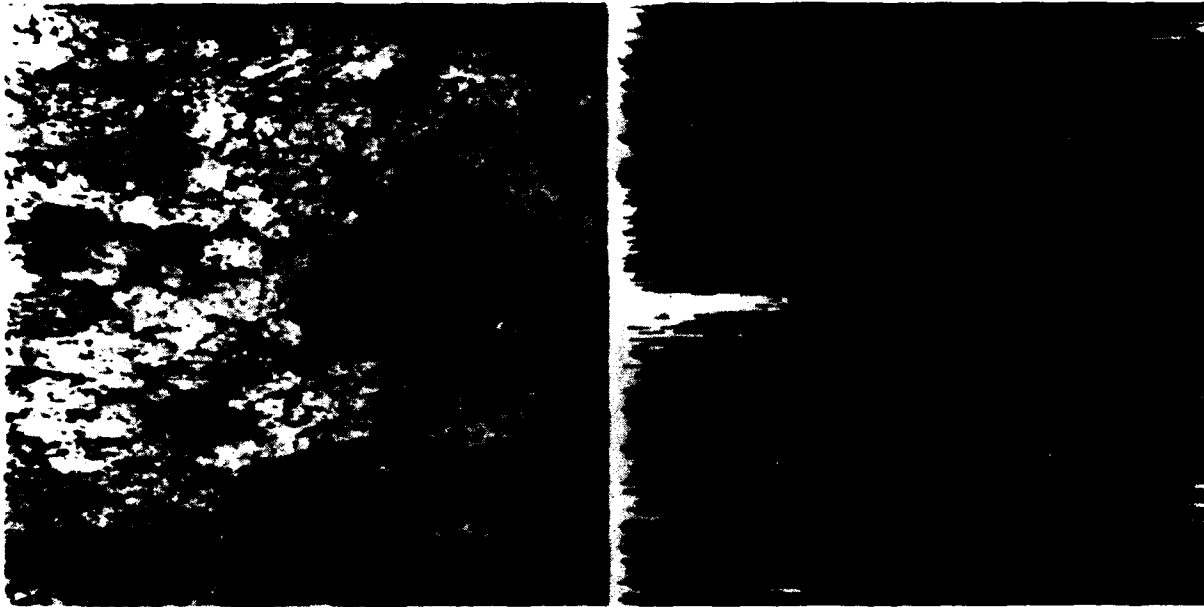


Scanner Data

Auto-Correlation

1356 - WEST - Ch 12 - at 350 ft

Figure 29. Conditions as in Figure 28 except data are from a flight in the west direction

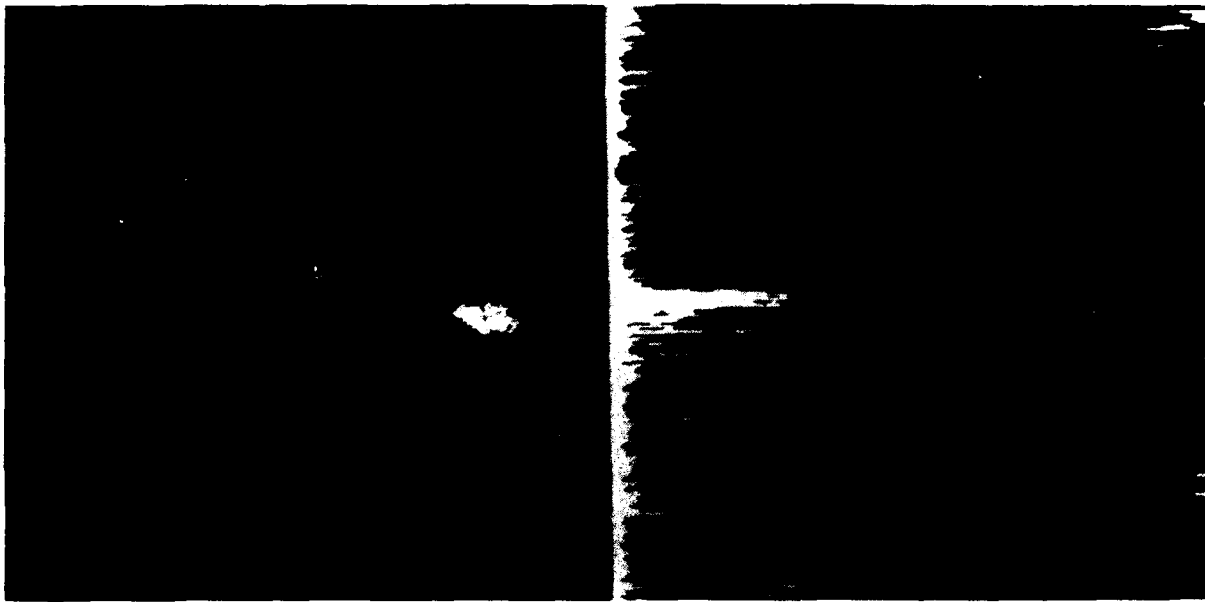


Scanner Data

Auto-Correlation

1356 - WEST - Ch 7 - at 350 ft

Figure 30. Conditions as in Figure 29 except data are channel 7



Scanner Data

Auto-Correlation

1356 - WEST - Ch 5 - at 350 ft

Figure 31. Conditions as in Figure 29 except data are from channel 5

Coherence length histogram for 0604 - Ch. 12 - West

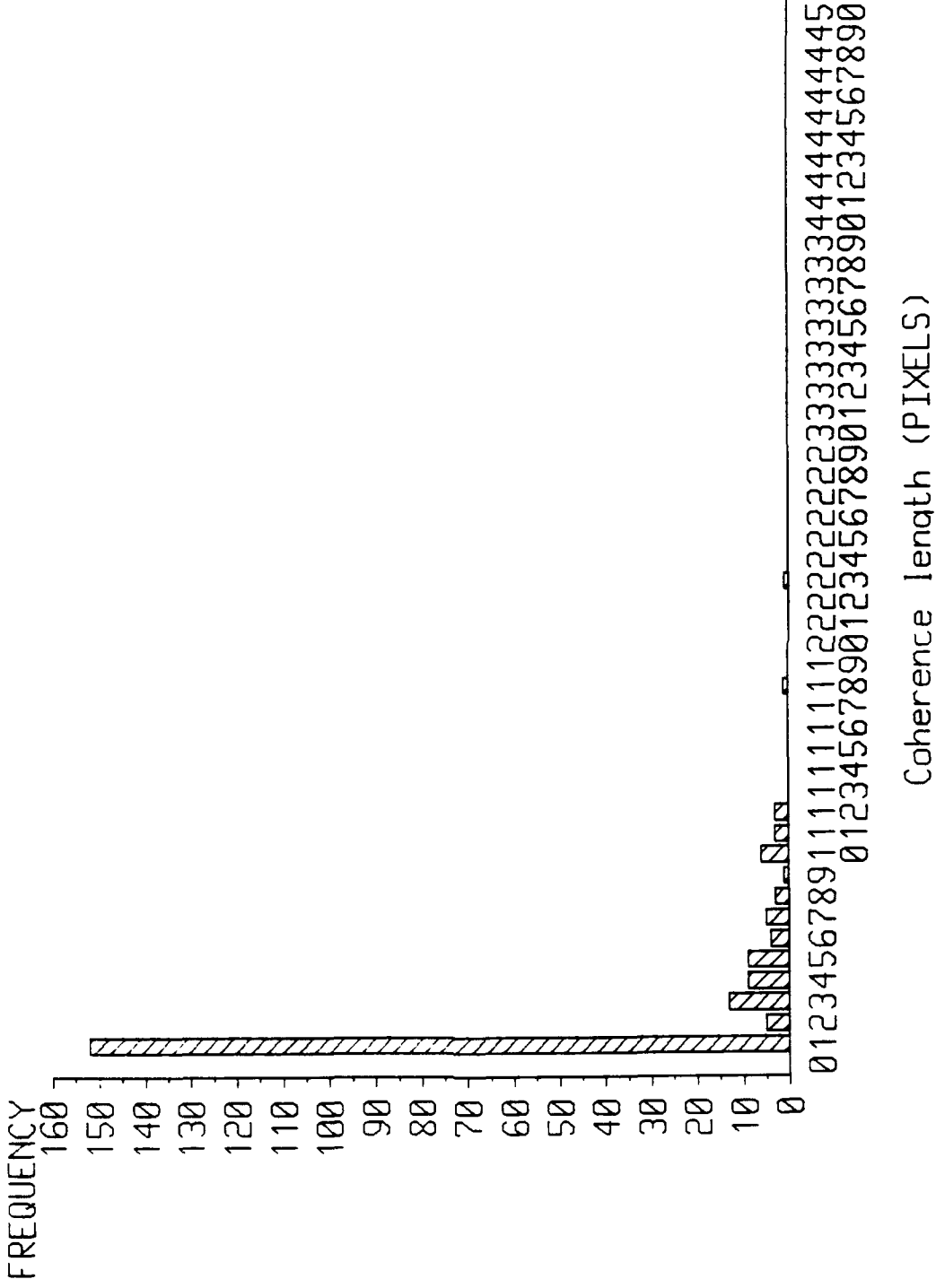


Figure 32. Histogram of coherence lengths for the predawn twilight thermal infrared data flown in the west direction at 350 ft agl

Coherence length histogram for 0931 -- Ch. 12 -- North

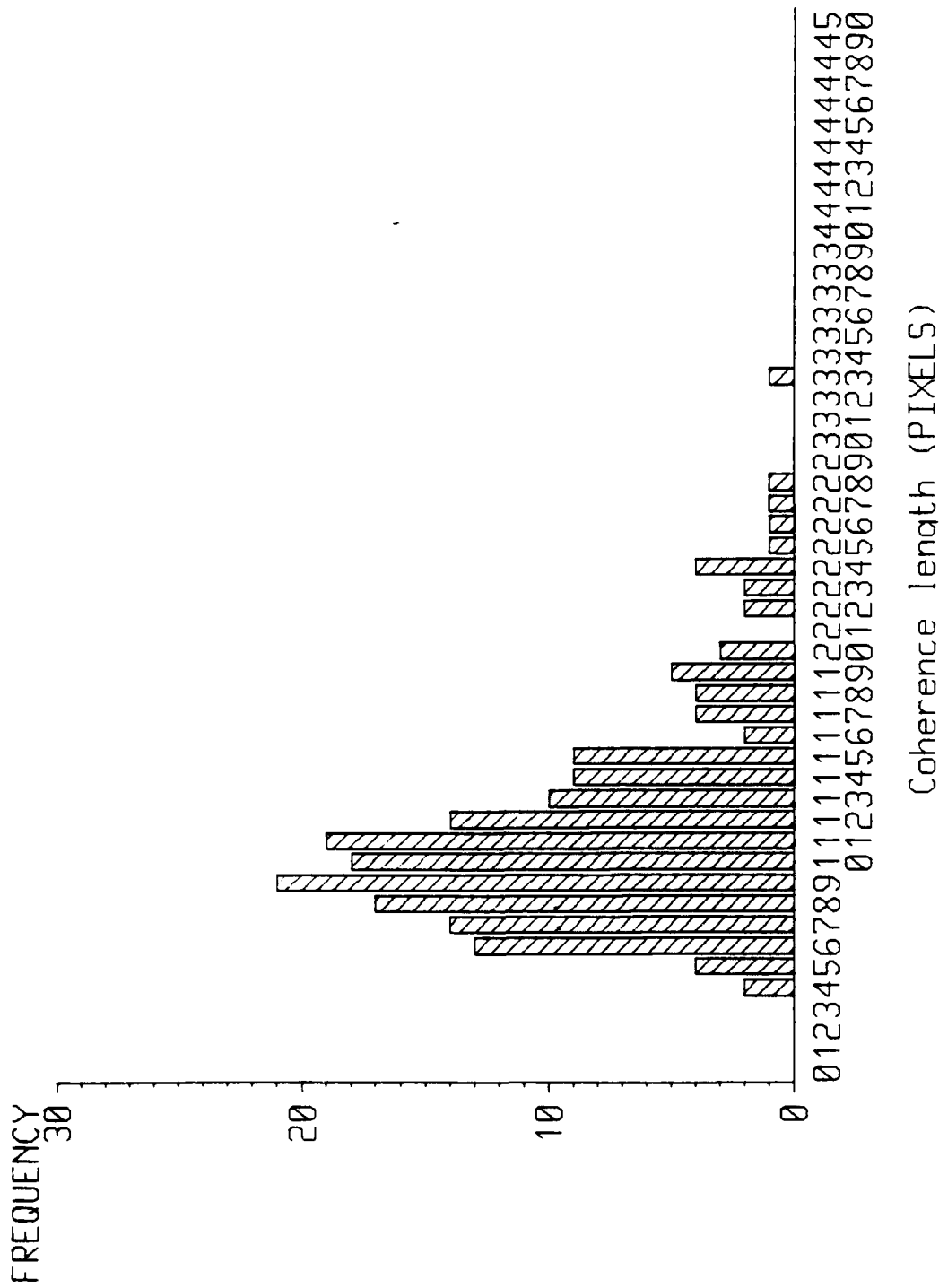


Figure 33. Conditions as in Figure 32 except data are from the midmorning north flight at 175 ft agl

Coherence length histogram for 0945 - Ch. 12 - West

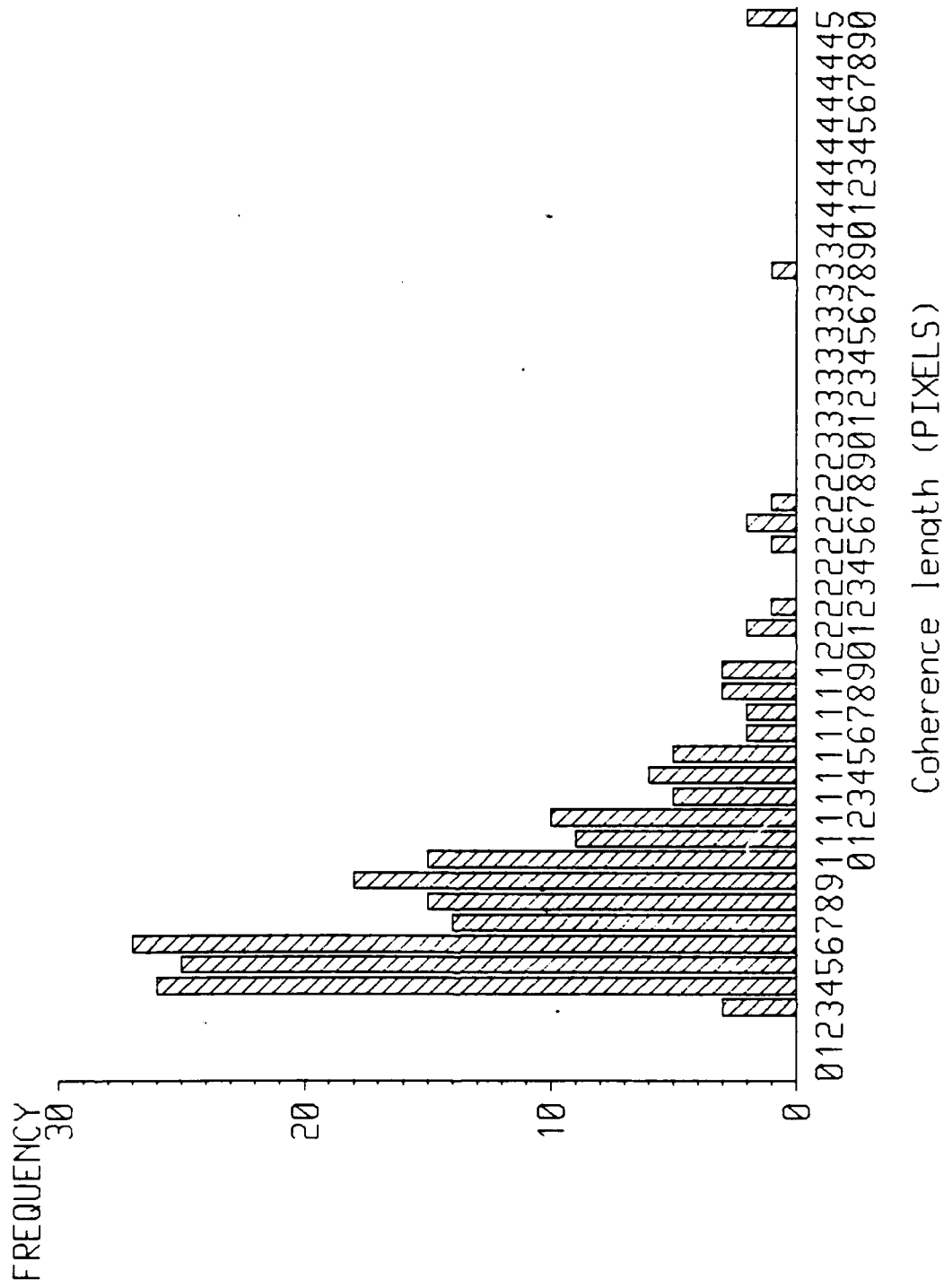


Figure 34. Conditions as in Figure 32 except the flight is west at 350 ft agl

Coherence length histogram for 0945 - Ch. 7 - West

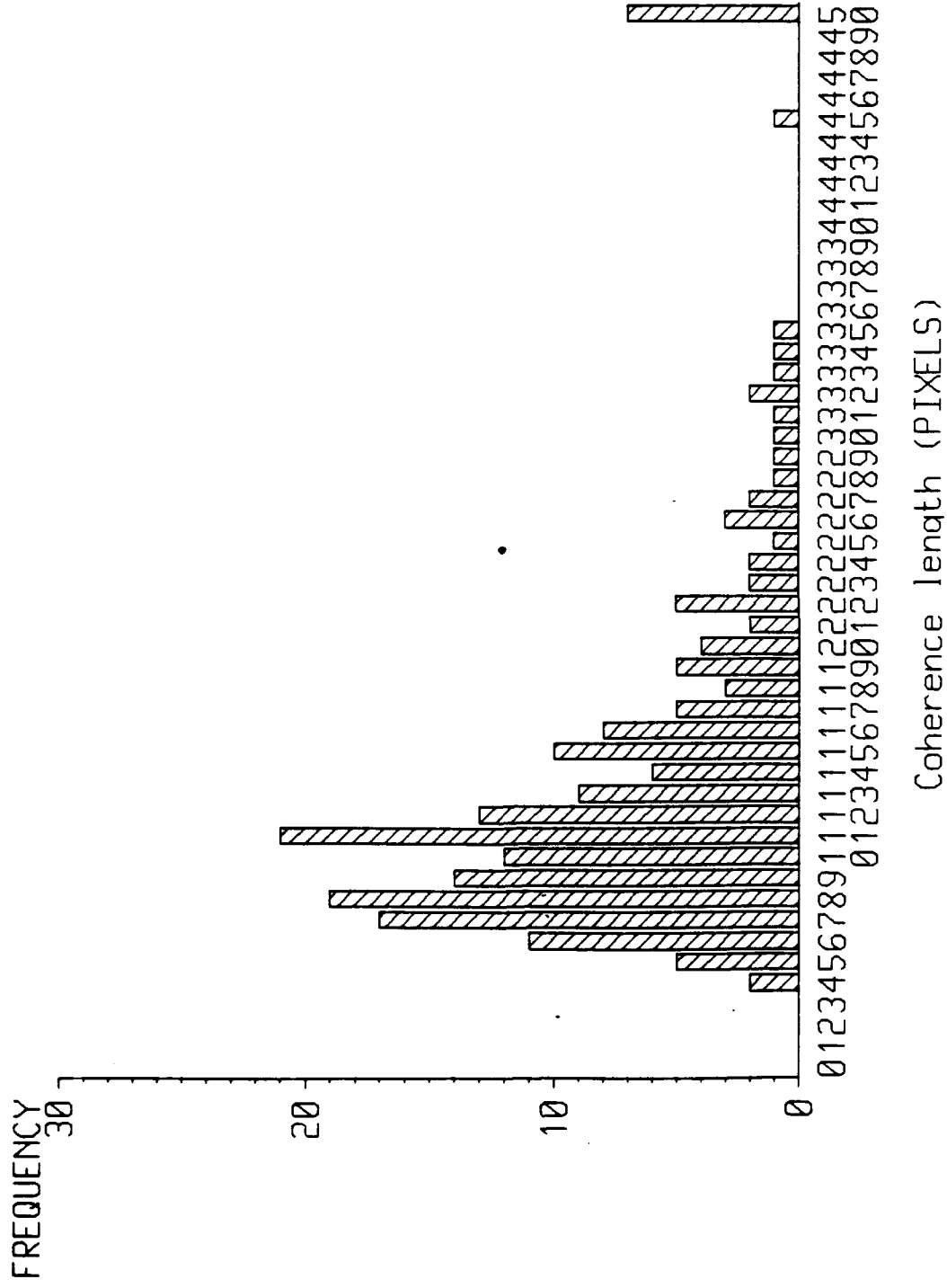


Figure 35. Conditions as in Figure 34 except the data are from channel 7

Coherence length histogram for 0945 - Ch. 5 - West

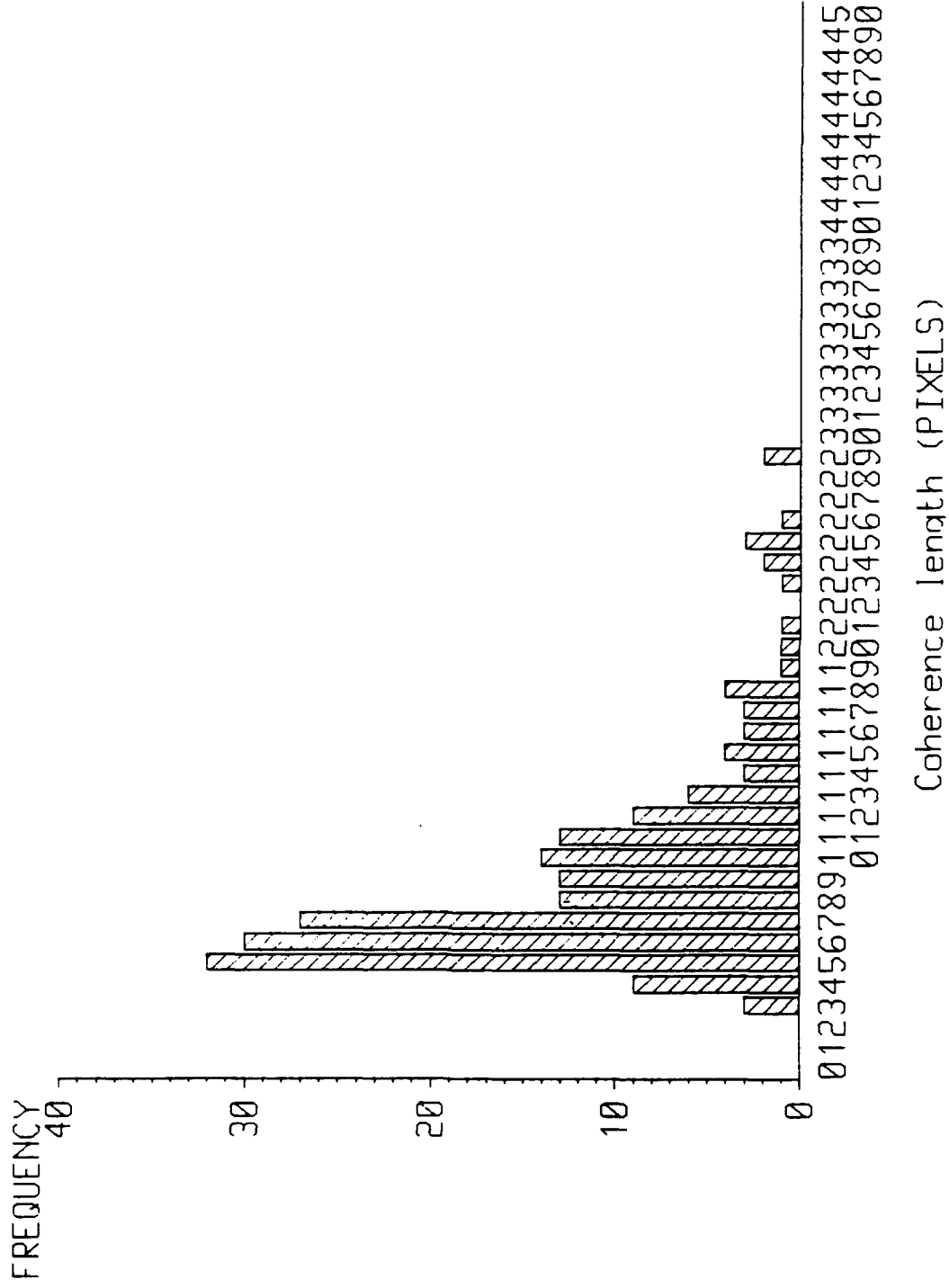


Figure 36. Conditions as in Figure 34 except data are from channel 5

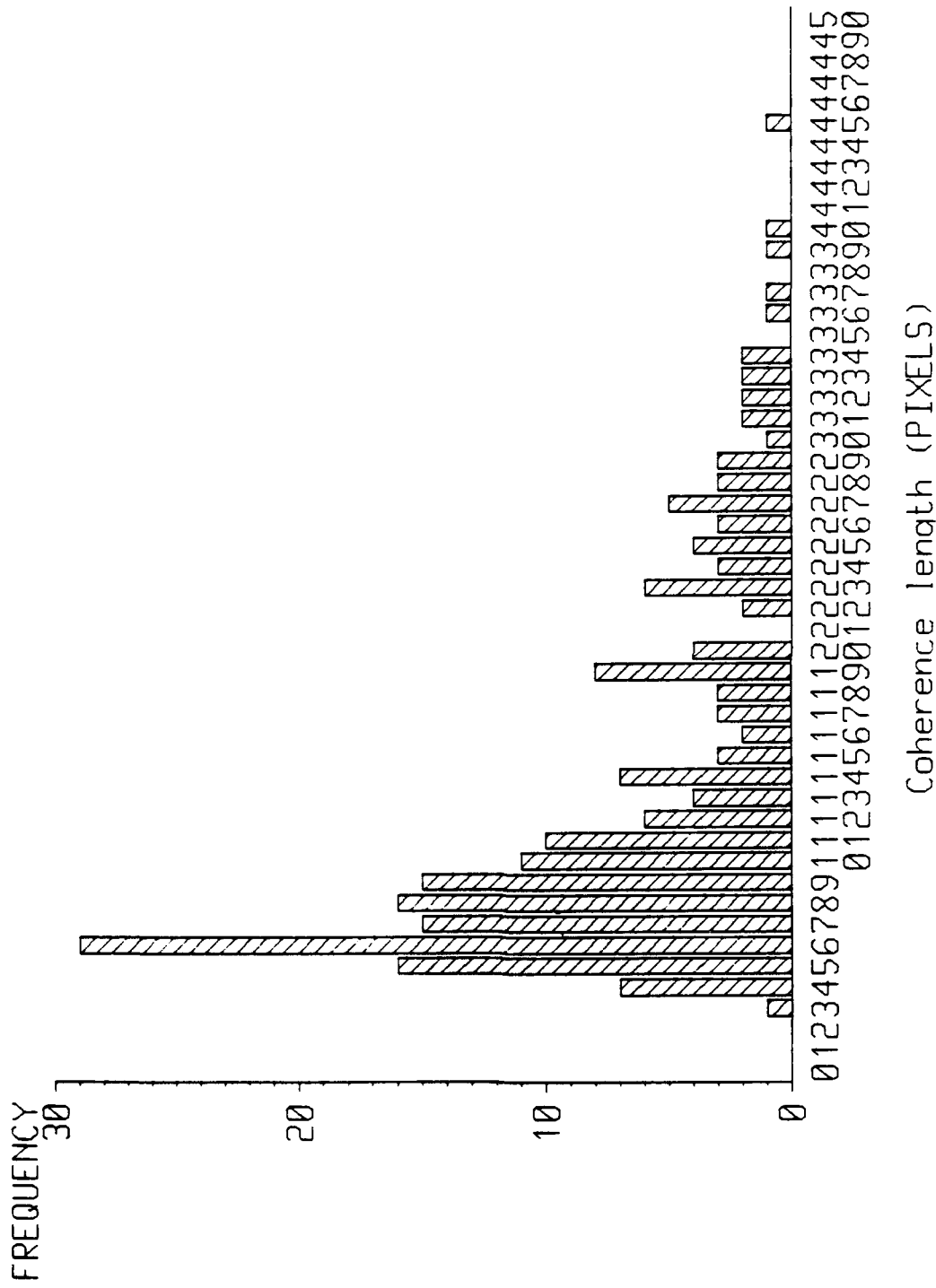


Figure 37. Conditions as in Figure 33 except data are taken near solar noon and the flight altitude is 350 ft agl

Coherence length histogram for 1356 - Ch. 12 - West

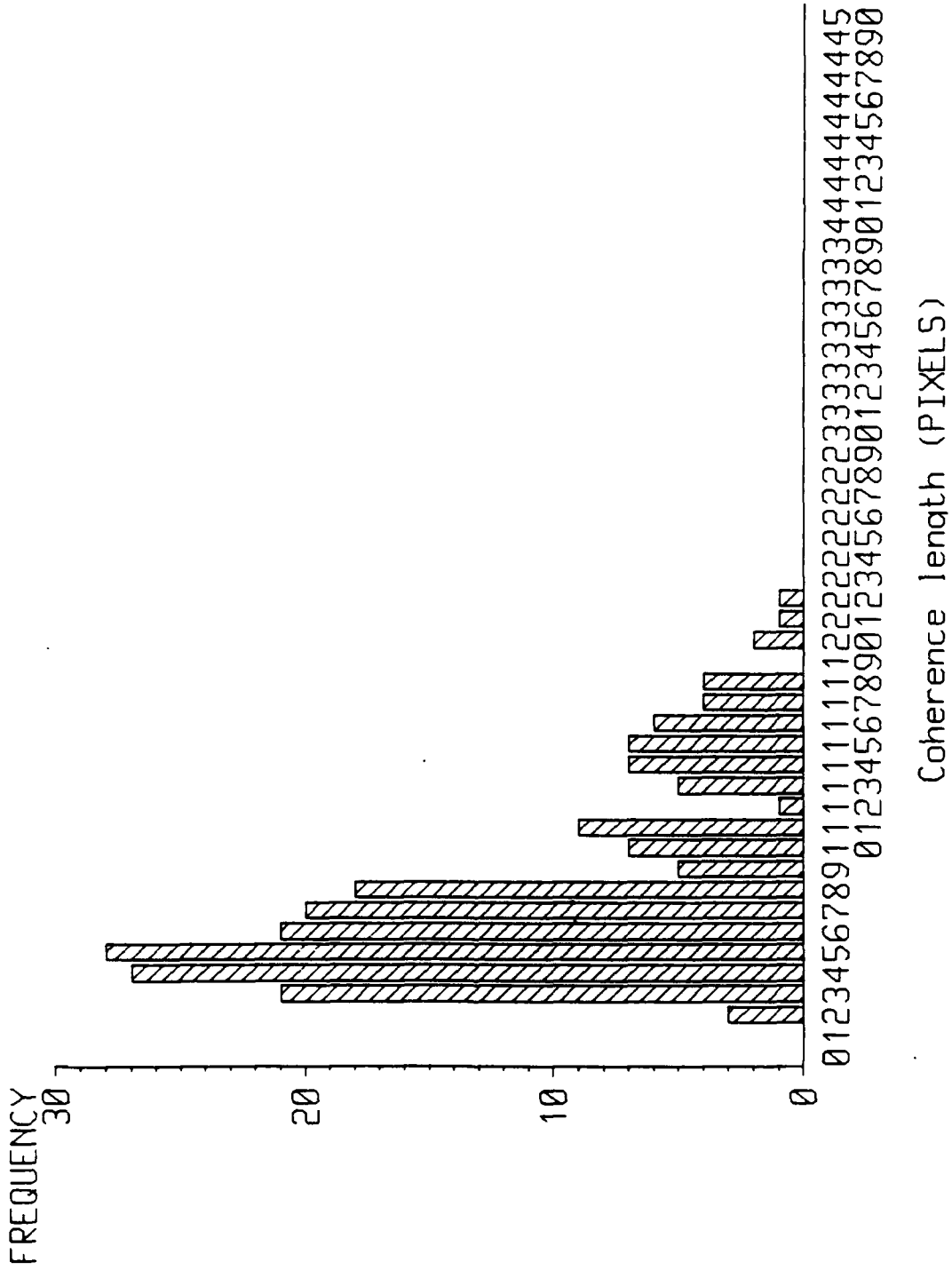


Figure 38. Conditions as in Figure 37 except the flight direction is west

Coherence length histogram for 1356

- Ch. 7 - West

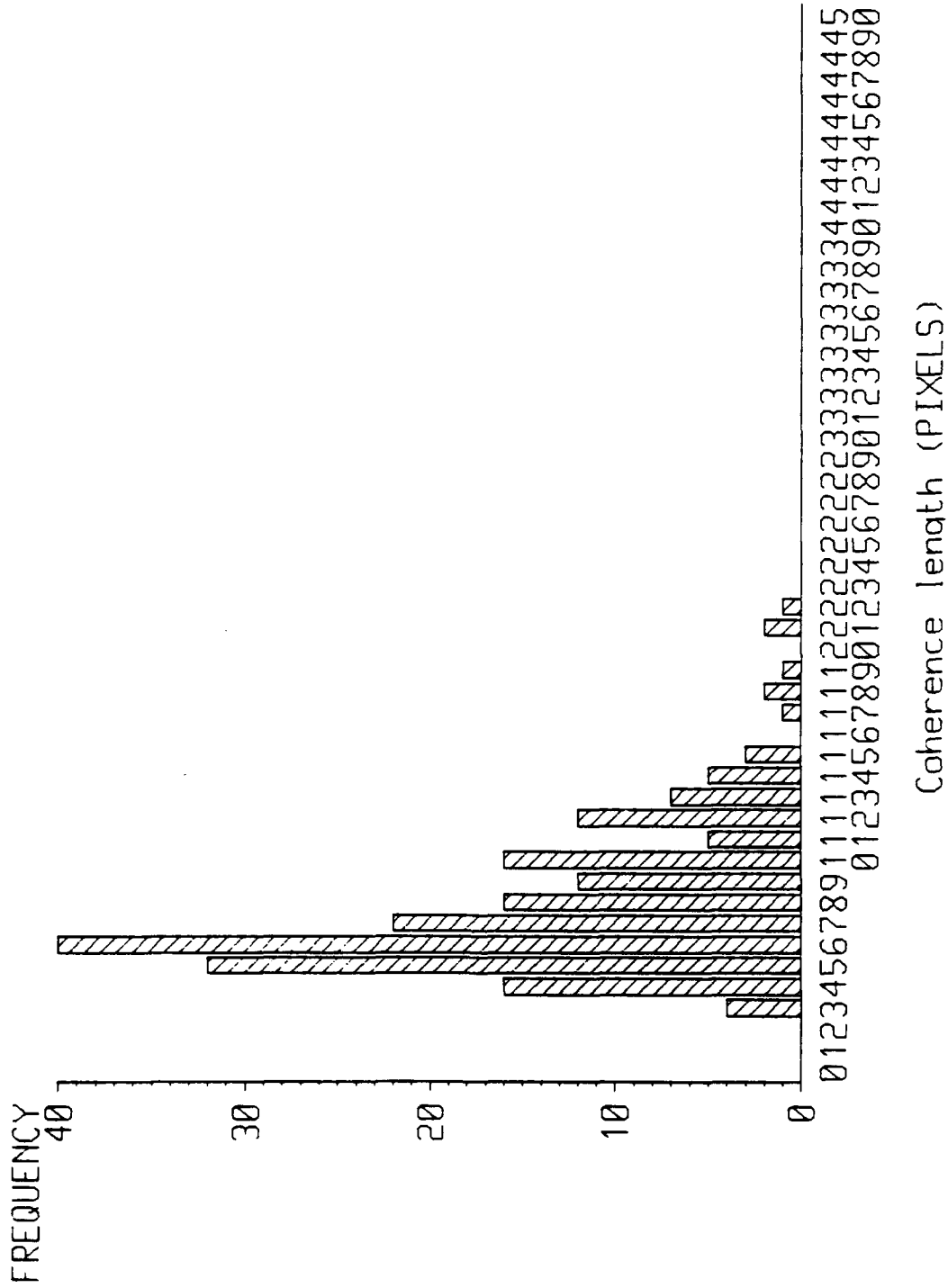


Figure 39. Conditions as in Figure 38 except data are from channel 7

Coherence length histogram for 1356

- Ch. 5 - West

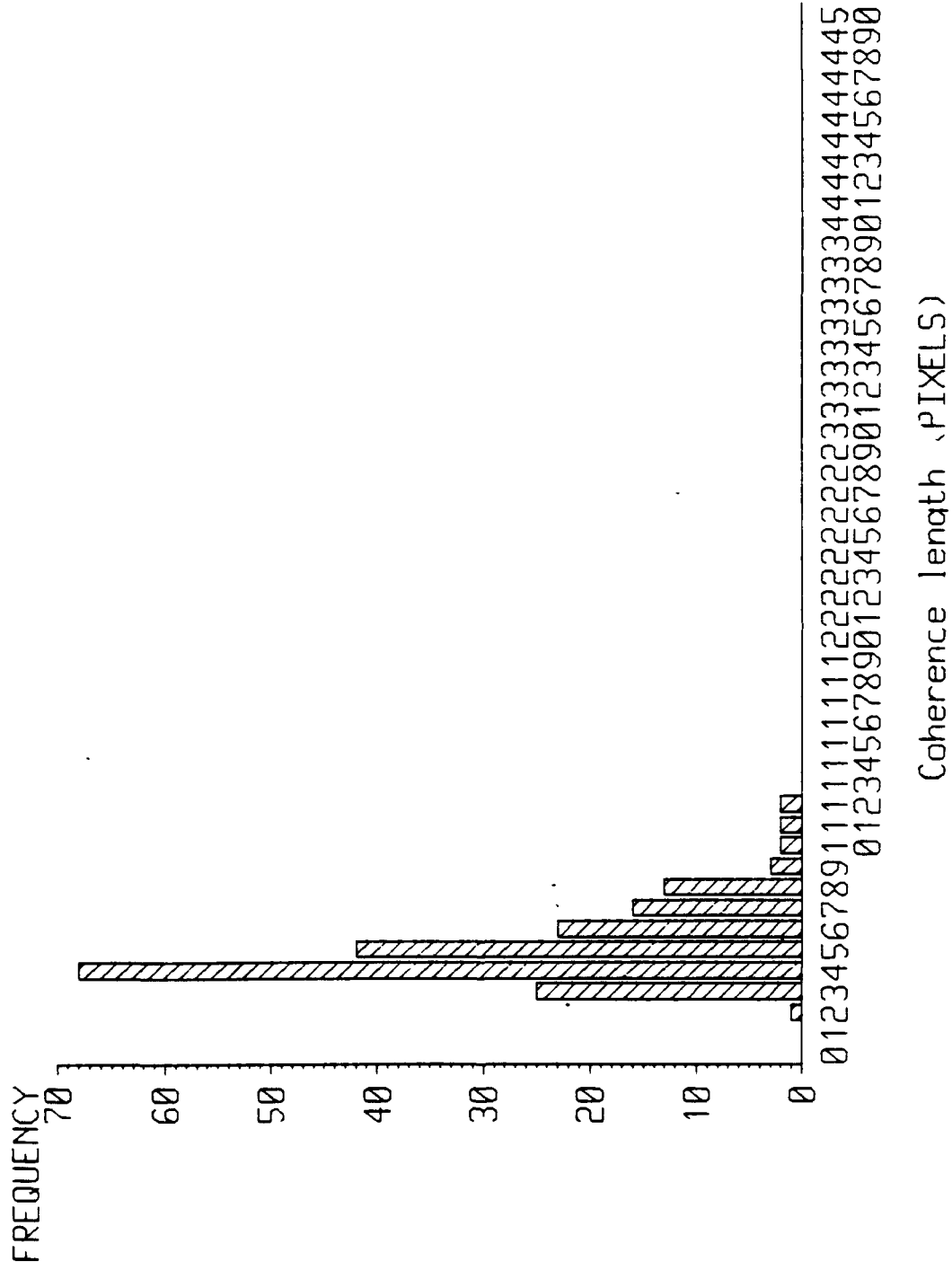
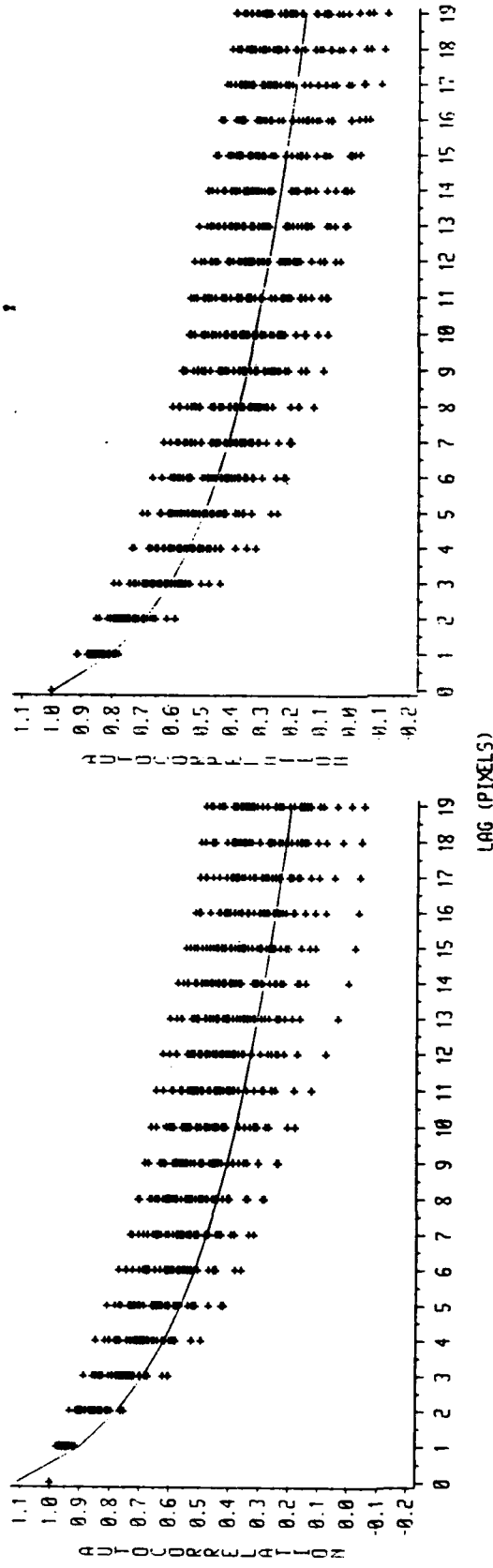


Figure 40. Conditions as in Figure 38 except data are from channel 5

Time : 0942 - Ch. 7 - North

Time : 1338 - Ch. 12 - North

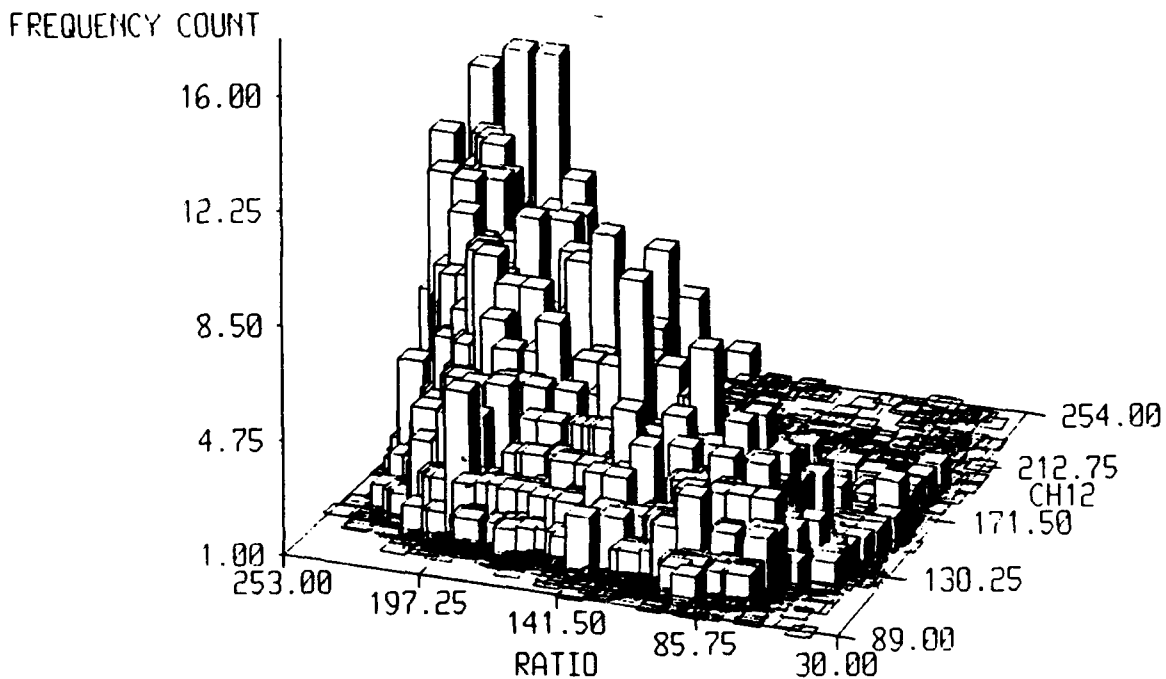


a. Midmorning north flight at 350 ft agl channel 7

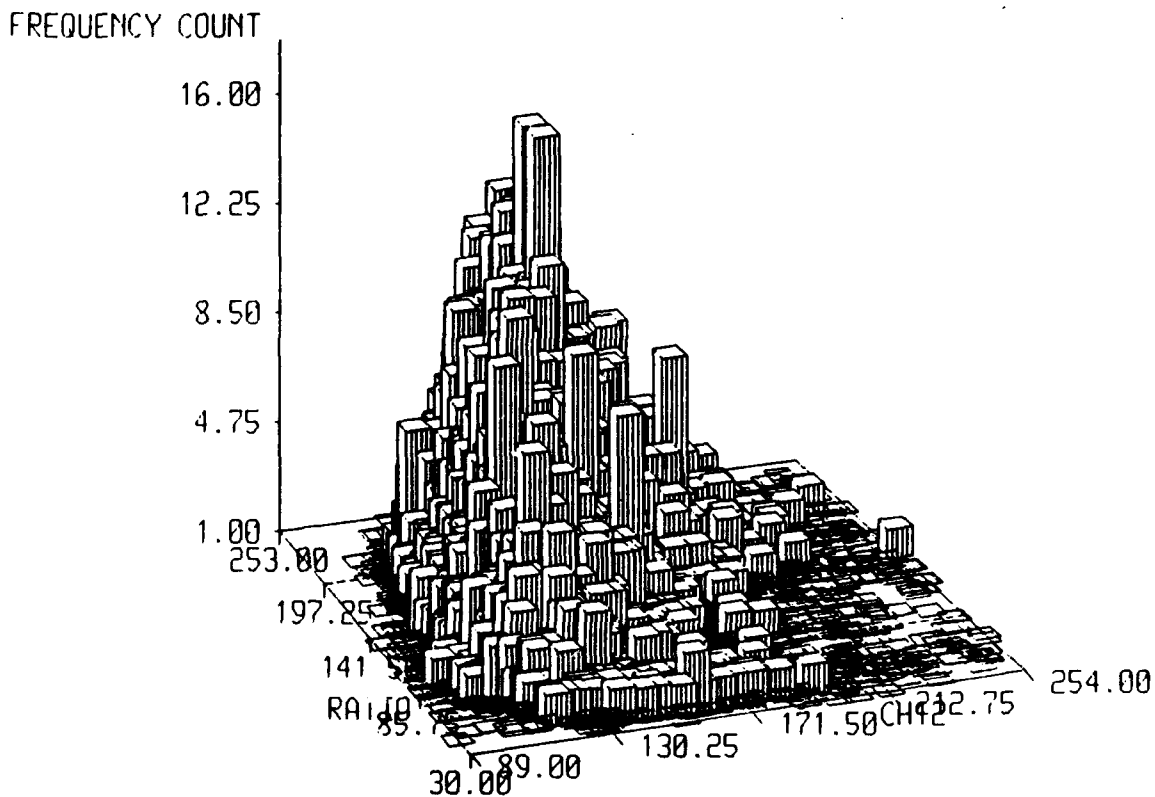
b. Midmorning north flight at 175 ft agl near solar noon in channel 12

Figure 41. Scattergrams of the first 20 points of the one-dimensional autocorrelation function of the first 50 scan lines of analyzed image data. Curves are plots of least square regression equations fit to the first 20 points in all the autocorrelation functions from all the analyzed data

3D histogram for 1353 - Ch. 12 vs 7:5 North



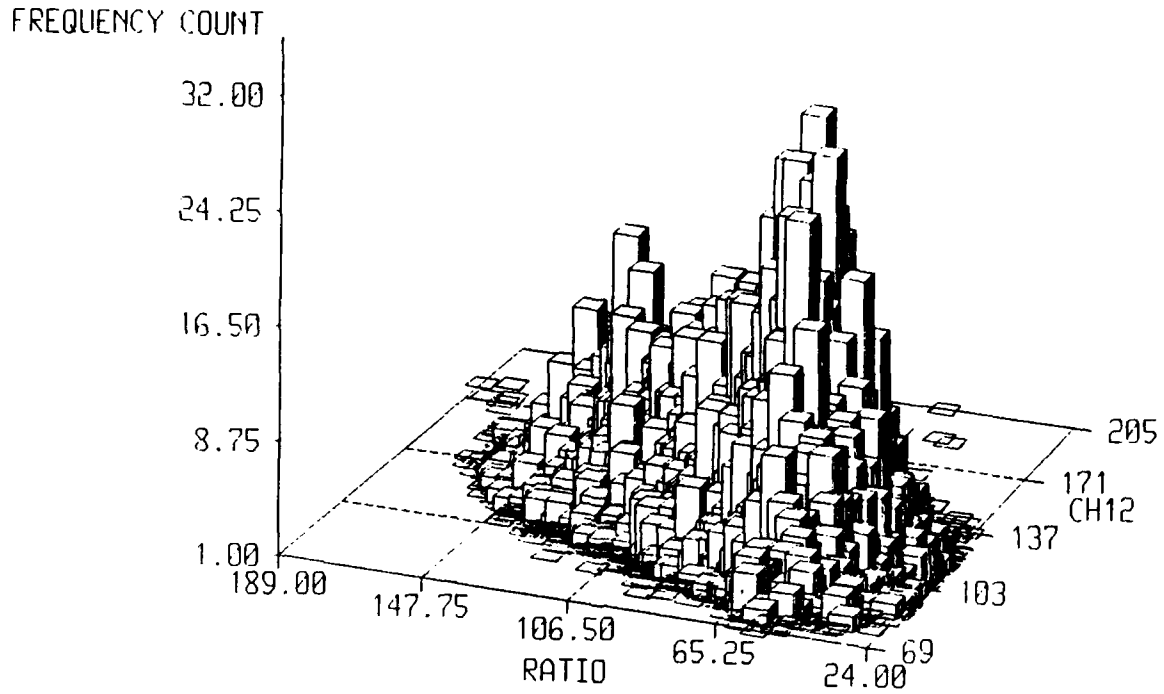
a.



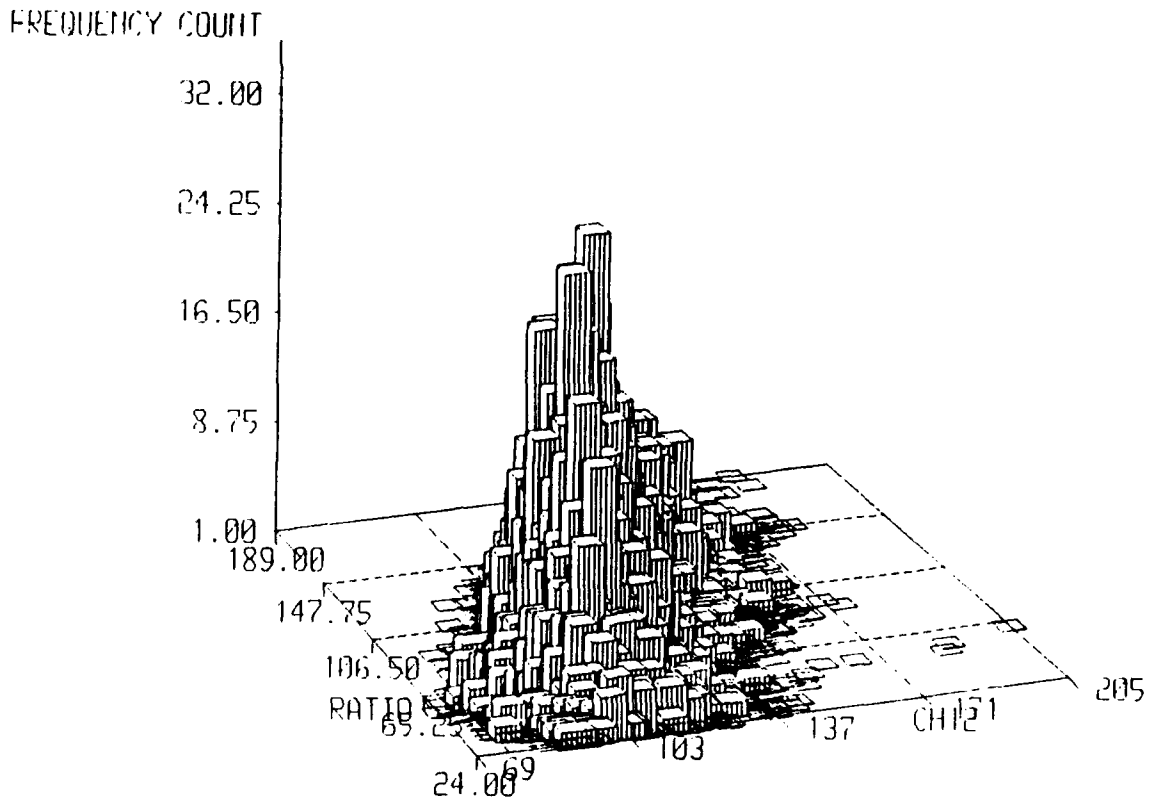
b.

Figure 42. Two views of the two-dimensional histogram of DNs of channel 5 versus channel 12 from the midmorning, north, 350 ft agl flight

3D histogram for 0942 - Ch. 12 vs 7/5 - North



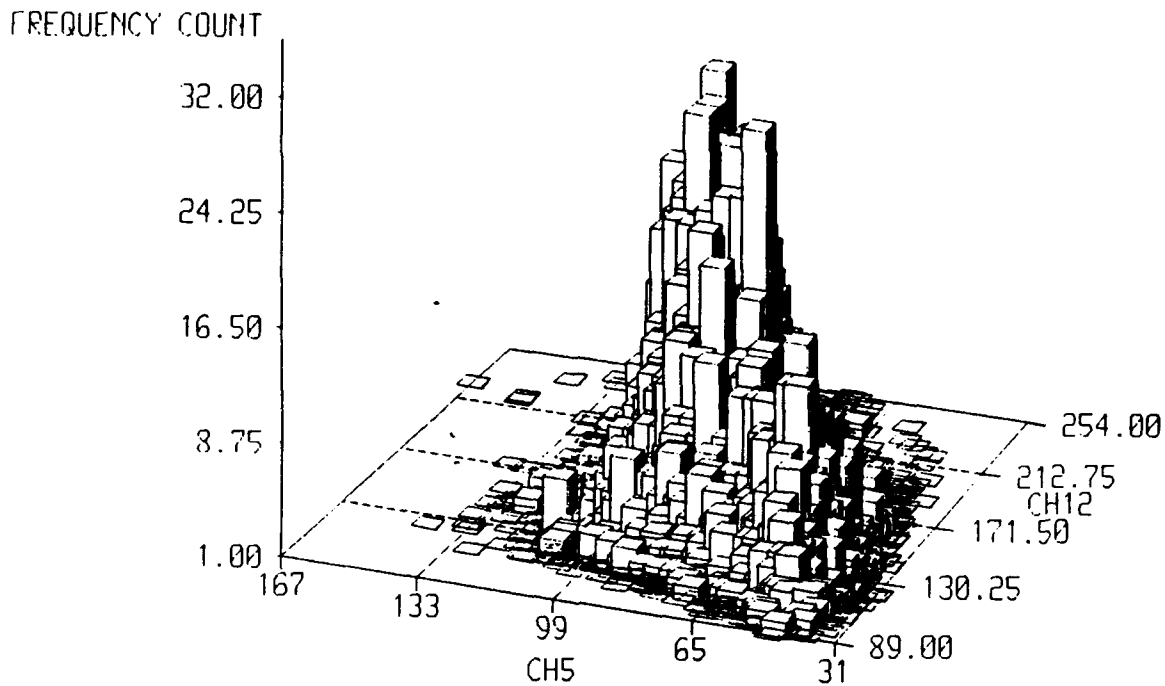
a.



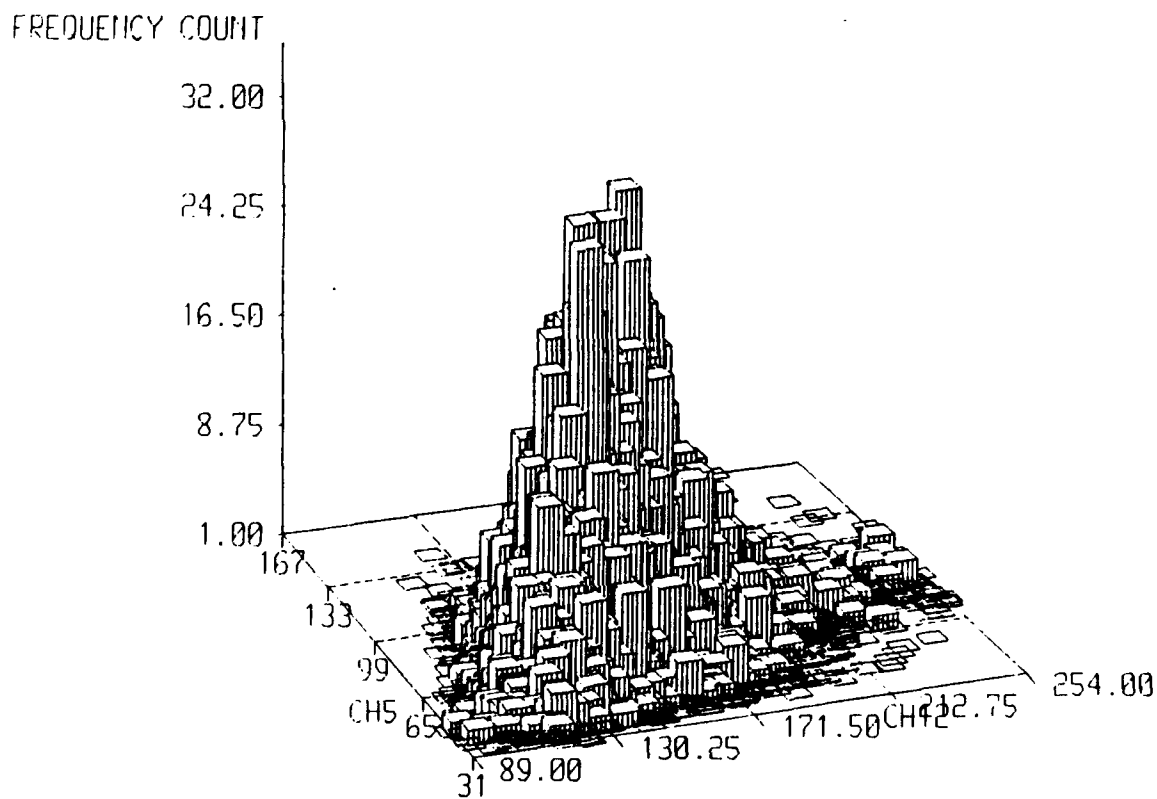
b.

Figure 43. Conditions as in Figure 42 except data are from the north, 350 ft agl flight near solar noon

3D histogram for 1353 - Ch. 12 vs 5 - North



a.

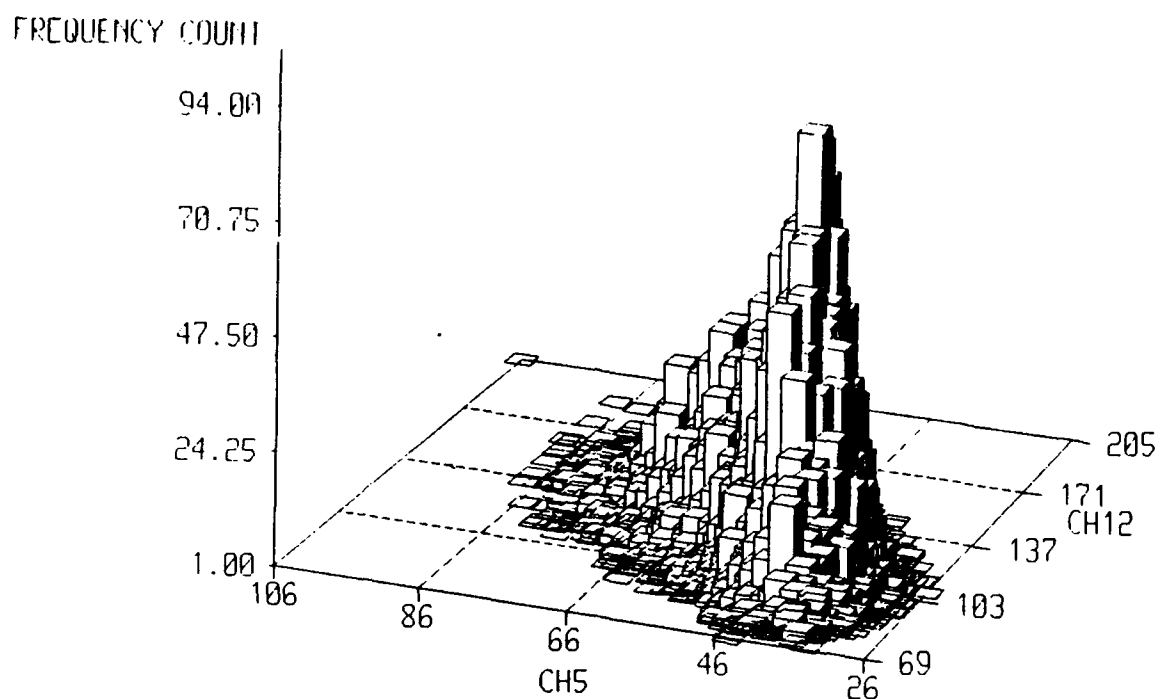


b.

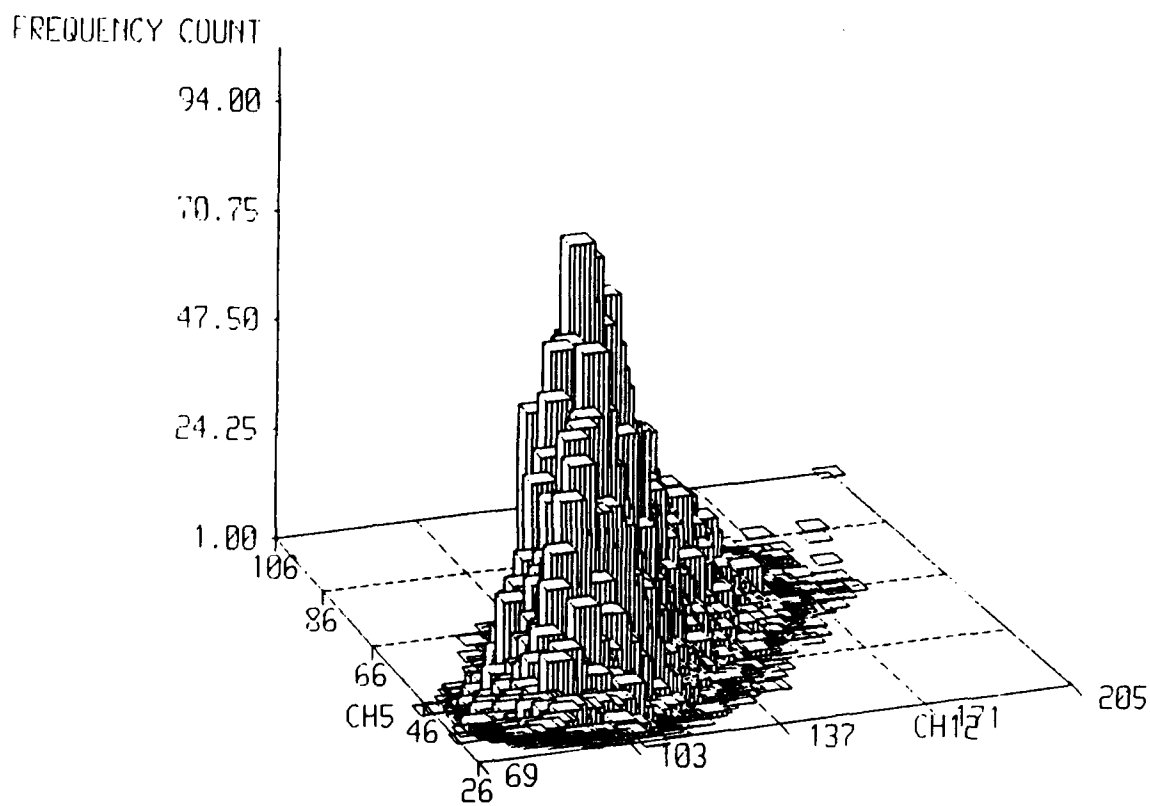
Figure 44. Conditions as in Figure 42 except the histogram is the DN7/DN5 ratio versus channel 12

3D histogram for 0942

Ch. 12 vs 5 North



a.



b.

Figure 45. Conditions as in Figure 43 except the histogram is the DN7/DN5 ratio versus channel 12

Waterways Experiment Station Cataloging-in-Publication Data

Balick, Lee K.

Deciduous forest scene complexity in high-resolution multispectral scanner imagery / by Lee K. Balick.

83 p. : ill. ; 28 cm. — (Technical report ; EL-92-26)

Includes bibliographic references.

1. Plant canopies — Tennessee — Remote sensing. 2. Spectrum analysis. 3. Infrared horizon sensors. 4. Scanning systems. I. Title. II. U.S. Army Engineer Waterways Experiment Station. III. Technical report (U.S. Army Engineer Waterways Experiment Station) ; EL-92-26.

TA7 W34 no.EL-92-26